CD8 + T cells are essential for the effects of enriched environment on hippocampus-dependent behavior, hippocampal neurogenesis and synaptic plasticity

Hadi Zarif, Sarah Nicolas, Mélanie Guyot, Salma Hosseiny, Anne Lazzari, María Magdalena Canali, Julie Cazareth, Frédéric Brau, Valentine Golzné, Elisa Dourneau, et al.

▶ **To cite this version:**

Hadi Zarif, Sarah Nicolas, Mélanie Guyot, Salma Hosseiny, Anne Lazzari, et al.. CD8 + T cells are essential for the effects of enriched environment on hippocampus-dependent behavior, hippocampal neurogenesis and synaptic plasticity. Brain, Behavior, and Immunity, 2018, 69, pp.235-254. 10.1016/j.bbi.2017.11.016 . hal-02269093

HAL Id: hal-02269093
https://hal.science/hal-02269093v1

Submitted on 22 Aug 2019

HAL is a multi-disciplinary open access archive for the deposit and dissemination of scientific research documents, whether they are published or not. The documents may come from teaching and research institutions in France or abroad, or from public or private research centers.

L'archive ouverte pluridisciplinaire **HAL**, est destinée au dépôt et à la diffusion de documents scientifiques de niveau recherche, publiés ou non, émanant des établissements d'enseignement et de recherche français ou étrangers, des laboratoires publics ou privés.

Accepted Manuscript

$CD8^+$ T cells are essential for the effects of enriched environment on hippocampus-dependent behavior, hippocampal neurogenesis and synaptic plasticity

Hadi Zarif, Sarah Nicolas, Mélanie Guyot, Salma Hosseiny, Anne Lazzari, María Magdalena Canali, Julie Cazareth, Frédéric Brau, Valentine Golzné, Elisa Dourneau, Maud Maillaut, Carmelo Luci, Agnès Paquet, Kevin Lebrigand, Marie-Jeanne Arguel, Douglas Daoudlarian, Catherine Heurteaux, Nicolas Glaichenhaus, Joëlle Chabry, Alice Guyon, Agnès Petit-Paitel

PII: S0889-1591(17)30517-2
DOI: https://doi.org/10.1016/j.bbi.2017.11.016
Reference: YBRBI 3287

To appear in: *Brain, Behavior, and Immunity*

Received Date: 18 July 2017
Revised Date: 13 November 2017
Accepted Date: 20 November 2017

Please cite this article as: Zarif, H., Nicolas, S., Guyot, M., Hosseiny, S., Lazzari, A., Magdalena Canali, M., Cazareth, J., Brau, F., Golzné, V., Dourneau, E., Maillaut, M., Luci, C., Paquet, A., Lebrigand, K., Arguel, M-J., Daoudlarian, D., Heurteaux, C., Glaichenhaus, N., Chabry, J., Guyon, A., Petit-Paitel, A., $CD8^+$ T cells are essential for the effects of enriched environment on hippocampus-dependent behavior, hippocampal neurogenesis and synaptic plasticity, *Brain, Behavior, and Immunity* (2017), doi: https://doi.org/10.1016/j.bbi.2017.11.016

This is a PDF file of an unedited manuscript that has been accepted for publication. As a service to our customers we are providing this early version of the manuscript. The manuscript will undergo copyediting, typesetting, and review of the resulting proof before it is published in its final form. Please note that during the production process errors may be discovered which could affect the content, and all legal disclaimers that apply to the journal pertain.

ACCEPTED MANUSCRIPT

$CD8^+$ T cells are essential for the effects of enriched environment on hippocampus-dependent behavior, hippocampal neurogenesis and synaptic plasticity

Hadi Zarif [1], Sarah Nicolas [1], Mélanie Guyot [2], Salma Hosseiny [1], Anne Lazzari [2], María Magdalena Canali [2], Julie Cazareth [1], Frédéric Brau [1], Valentine Golzné [1], Elisa Dourneau [1], Maud Maillaut [1], Carmelo Luci [3], Agnès Paquet [1], Kevin Lebrigand [1], Marie-Jeanne Arguel [1], Douglas Daoudlarian [2], Catherine Heurteaux [1], Nicolas Glaichenhaus [2], Joëlle Chabry [2$], Alice Guyon [1*$] & Agnès Petit-Paitel [1*]

1- Université Côte d'Azur, CNRS, IPMC, France

2- Université Côte d'Azur, INSERM, CNRS, IPMC, France

3- Université Côte d'Azur, C3M, INSERM U 1065, France

* Co-direction of the work

$ Corresponding authors

Present address: Alice GUYON

IPMC CNRS UMR 7275, 660 route des Lucioles

06560 Valbonne, France

Email : alice.guyon@ipmc.cnrs.fr

Joëlle Chabry

IPMC CNRS UMR 7275, 660 route des Lucioles

06560 Valbonne, France

Email : joelle.chabry@ipmc.cnrs.fr

ACCEPTED MANUSCRIPT

Highlights:

- $CD8^+$ T cells play a major role in brain plasticity changes that are induced by an enriched environment in mice, as revealed by behavioral experiments and measurements of hippocampal volume, neurogenesis in the dentate gyrus of the hippocampus, spinogenesis and glutamatergic synaptic function in cornu ammonis (CA) of the hippocampus.

- Peripheral $CD8^+$ T cells have different properties in mice raised in an enriched environment (EE) as compared to mice raised in a standard environment (SE). Spleen $CD8^+$ T cells from SE vs EE mice are different in terms of 1) cytokine release after *in vitro* stimulation 2) *in vitro* proliferation properties 3) $CD44^+$ $CD8^+$ $CD62L^{low}$ and $CD62L^{hi}$ T cell proportions and 4) transcriptomic signature as revealed by RNA sequencing.

- $CD8^+$ T cell ratios and repartition of effector and central memory $CD8^+$ T cells differ between spleen and brain. Brain $CD8^+$ T cell transcriptomic signatures are differentially modified by EE housing, in comparison to peripheral $CD8^+$ T cells.

Keywords:

Enriched environment, $CD8^+$ T cells, hippocampus, brain plasticity, behavior, neurogenesis, synaptogenesis, long term potentiation, choroid plexus, mice

ACCEPTED MANUSCRIPT

Abstract

Enriched environment (EE) induces plasticity changes in the brain. Recently, $CD4^+$ T cells have been shown to be involved in brain plasticity processes. Here, we show that $CD8^+$ T cells are required for EE-induced brain plasticity in mice, as revealed by measurements of hippocampal volume, neurogenesis in the DG of the hippocampus, spinogenesis and glutamatergic synaptic function in the CA of the hippocampus. As a consequence, EE-induced behavioral benefits depend, at least in part, on $CD8^+$ T cells. In addition, we show that spleen $CD8^+$ T cells from mice housed in standard environment (SE) and EE have different properties in terms of 1) TNFα release after *in vitro* CD3/CD28 or PMA/Iono stimulation 2) *in vitro* proliferation properties 3) $CD8^+$ $CD44^+$ $CD62L^{low}$ and $CD62L^{hi}$ T cells repartition 4) transcriptomic signature as revealed by RNA sequencing. $CD8^+$ T cells purified from the choroid plexus of SE and EE mice also exhibit different transcriptomic profiles as highlighted by single-cell mRNA sequencing. We show that $CD8^+$ T cells are essential mediators of beneficial EE effects on brain plasticity and cognition. Additionally, we propose that EE differentially primes $CD8^+$ T cells leading to behavioral improvement.

ACCEPTED MANUSCRIPT

ACCEPTED MANUSCRIPT

INTRODUCTION

Environmental enrichment (EE) refers to housing conditions, such as home cages or exploratory chambers that facilitate enhanced sensory, cognitive and motor stimulation. EE housing induces structural changes in the brain, i.e. plasticity, and more specifically in the hippocampus which is primarily involved in spatial learning, memory and mood regulation. We have previously shown that housing mice in EE for 4 weeks increased neurogenesis in the dentate gyrus (DG) of the hippocampus, induced changes in neuronal morphology, and modified synaptic plasticity (Hosseiny et al., 2015). Compared to mice housed in a standard environment (SE), EE mice exhibited an increased number of functional synapses as demonstrated by measuring spontaneous and miniature excitatory post synaptic currents (EPSCs) recorded on CA1 neurons, larger field excitatory postsynaptic potential (fEPSPs) and decreased long term potentiation (LTP).

The immune system is primarily involved in protection from infectious agents. However, studies performed over the past 30 years have demonstrated that it is also involved in neurobehavioral processes. For example, cytokines produced by immune cells in infected individuals induce sickness behavior and impaired neurobehavioral plasticity. Furthermore, because both glia and neurons express cytokines and their receptors in the absence of infection, it was suggested that cytokines could act as neuromodulators to regulate brain function in non-pathological conditions (Donzis and Tronson, 2014; Vitkovic et al., 2000; Yirmiya and Goshen, 2011). Indeed, cytokines were shown to have a critical role in sleep (Krueger et al., 2001; Opp, 2005; Wolf et al., 2003). Furthermore, studies using lymphocyte-deficient Severe Combined Immune Deficiency (SCID) mice and T cell-deficient nude mice have demonstrated the critical role of T cells in brain function. SCID mice display dramatic impairments in hippocampal-dependent spatial learning and memory assessed in spatial tasks such as the Morris water maze paradigm (Kipnis et al., 2004a; Kipnis et al., 2004b; Ron-Harel et al., 2008), the radial arm water maze (Brynskikh et al., 2008) and tests designed to

ACCEPTED MANUSCRIPT

assess recognition of the novel spatial arrangement of familiar objects (Ron-Harel et al., 2008). Likewise, $CD4^+$ T cell depletion results in impaired memory and learning, as well as decreased LTP and neurogenesis (Kipnis et al. 2004b). More recently, Schwartz, Kipnis and their colleagues have shown that auto-reactive $CD4^+$ T cells that recognized brain antigens could be neuroprotective (Kipnis et al., 2008; Schwartz and Kipnis, 2011; Schwartz and Shechter, 2011). While these latter studies clearly demonstrated a role of $CD4^+$ T cells in brain function, almost nothing is known about the role of $CD8^+$ T cells, and this despite the fact that $CD8^+$ T cells are in equal proportions or even outnumber $CD4^+$ T cells in both the human and the mouse brain (Bradl et al., 2005; Ritzel et al., 2016; Smolders et al., 2013; Song et al., 2016).

Here, we have investigated the role of $CD8^+$ T cells in EE-induced brain plasticity. We found that $CD8^+$ T cell depletion abolished EE-induced behavioral changes, hippocampal plasticity, neurogenesis in DG, spinogenesis in CA and functional synaptic plasticity in CA1. We further demonstrated that $CD8^+$ T cells in SE and EE mice were functionally different in both the spleen and the brain.

ACCEPTED MANUSCRIPT

ACCEPTED MANUSCRIPT

MATERIALS AND METHODS

1. Mouse strains and housing

C57BL6/J female mice (Janvier Labs, France) were exposed to EE starting 4 weeks after birth (i.e. at weaning) for a 1, 2, 3 or 4 week period (Suppl Fig 1 A and B). A total number of 388 C57BL6/J mice were used for this study. 12-15 age-matched mice were housed in large-sized cages (9120 cm^2; L x l x h: 120 x 76 x 21 cm) with nesting material, houses, running wheels, hammocks, scales, plastic toys and tunnels (Suppl Fig 1C). Objects were changed twice a week. Mice in standard conditions (SE) were housed in medium sized cages (666 cm^2; L x l x h: 36 x 18.5 x 14 cm) with 5-6 mice/cage without objects. All mice had access to tap water and standard lab chow (diet SAFE A04, 2900 kcal/kg) *ad libitum* and were housed in a 12 hr light/12 hr dark cycle at 22-23°C with 40-60% humidity. The animals analyzed in each experiment were randomized either in SE or EE.

20 OT-I female mice (Charles River, France) of the same age, raised in the same conditions, were also used for a set of experiments. These homozygous mice have a transgenic MHC class I-restricted alpha beta T cell receptor designed to recognize ovalbumin (OVA) residues 257-264, an antigen that is absent in the mouse.

All animal studies were carried out in accordance with French standard ethical guidelines for laboratory animals (Agreement N° 75-178, 05/16/2000) and the European Communities Council Directive of 24 Nov 1986 (86/609/EEC). Formal approval to conduct the experiments described has been obtained from the animal subjects review board of our institution and can be provided upon request. All efforts were made to minimize the number of animals used and their suffering.

2. T cell depletion

For T cell depletion, 3-week old C57BL6/J female mice were injected *ip* with 0.5 mg of anti-CD8α (clone 53-6.72, BioXCell or from hybridoma culture supernatants ATCC® No. TIB-105™), or

ACCEPTED MANUSCRIPT

isotype control (clone 2A3, BioXCell) mAb. We found that the anti-CD8 "depleting" antibody was in fact a neutralizing antibody and thus we had to use these antibodies together with mouse anti-rat secondary antibodies (IgG2b, clone RG9/6.13 HLK from hybridomas culture supernatant ATCC® No. TIB-167™) in order to obtain complete depletion 3 days post-injection as previously described (Goldschmidt et al., 1988) (Suppl Fig 2). 3 days after the first injection, mice were placed in either SE or EE. Mice received the second and third injections (0.3 mg), 10 days apart each, with the control groups receiving the control antibody at the same time. The mice were subsequently sacrificed, spleens were harvested and immune cells prepared to control for the absence of $CD8^+$ T cells by using flow cytometry with anti-CD3, anti-CD8 and anti-CD4 antibodies (BD Biosciences). No depletion was observed in control mice, while around 98% depletion was observed with the anti-CD8 antibody (Suppl Fig 2A). In order to confirm that the depleting antibodies were efficient in the brain, we measured the presence of T cells in the whole brain by FACS (LSRII Fortessa, BD Biosciences, Rungis) (Suppl Fig 2B).

3. Behavioral studies

Before each trial, all devices were thoroughly cleaned with 70% ethanol and dried. All behavioral tests were performed once on the same cohort of mice (N=9 per group), in order rotarod, L&D, OF, social interactions, NSF and FST one day apart. The behavioral tests were performed in this order owing to the increasing of stressfulness (Suppl Fig 1B). An independent cohort of mice N=10-14 per group was submitted to the Barnes maze experiment.

3.1 Rotarod

For assessing motor coordination, mice were placed on a rotating wheel for two 5 min-habituation phases on fixed rod (10 rpm/min) 4 hours apart. Twenty-four hours later, the latency to fall was recorded on accelerating rod (from 10 to 40 rpm/min). The retention duration on the rod was

ACCEPTED MANUSCRIPT

an index of motor coordination.

3.2 Open-field (OF) activity and light/dark (L&D) preference tests

Anxiety-like behavior was assessed using the OF and L&D preference tests as previously described (Bailey et al., 2009; Kinsey et al., 2007; Wohleb et al., 2011). For the OF test, mice were placed in the corner of the test apparatus (*40L*×*40W*×25*H* cm Plexiglas box, center area *20L*×*20W*) and activity was recorded for 5 min. Initially, 9 mice per group were tested, however some recording of the OF test were damaged and data were lost, explaining why the number of mice per groups was 6-9 (Figure 1B). Mice with anxiety-like behavior entered the center less often, delayed the first entry and spent less time in the center of the arena. For light/dark preference (L&D), the test apparatus (40*L* × 30*W* × 25*H* cm) was divided into two equal zones with a doorway connecting the two sides. The light zone was very bright (500-600 lux) while the dark zone was protected from light by an opaque lid. To initiate testing, mice were placed into the light side and activity was recorded for 5 min.

3.3 Novelty suppressed feeding (NSF)

NSF is a conflict test that elicits competing motivation: the drive to eat and the fear of venturing into the center of the brightly lit arena. The testing apparatus consisted of a plastic box (45*L* × 45*W* × 25*H* cm) with 2 cm of wooden bedding on the floor and a single pellet of food in the center. Mice were fasting for 20 h prior testing. At the time of testing, an animal was placed in a corner of the box, and the entire session was videotaped (i.e. 10 min period). The latency to eat (defined as the mouse sitting on its haunches and biting the pellet) was timed. Immediately after the test, food consumption was measured for 5 min as control for potential feeding differences.

3.4 Forced swimming test (FST)

ACCEPTED MANUSCRIPT

Mice were placed in a glass bucket (20 cm diameter, 30 cm deep, filled with water 23°C ± 0.5°C). As described previously by (Porsolt et al., 1977), only the last 4 min were scored for immobility duration. A mouse was considered immobile when it remained floating in an upright position with only slight movements to keep its head above water (Pechnick et al., 2004).

3.5 Social interaction test

The social testing apparatus was a rectangular, three-chambered box with clear Plexiglas walls, having small circular openings (3.5 cm in diameter) allowing access into each chamber (25Lx15Wx20H cm). Three interconnected chambers were separated by manually operated sliding doors. The test mouse was first placed in the middle chamber and allowed to explore the entire apparatus for five minutes under dim light (25 lux). During the habituation period, the chambers were empty. At the end of the session, the test mouse was confined into the center chamber for two minutes by obstruction of the doorways between the two side chambers. An unfamiliar C57BL/6J female in same age range, that had no prior contact with the subject mice, was enclosed in a perforated box of one of the side chambers while another empty perforated box was placed in the opposite chamber. Both doors to the side chambers were then unblocked and the test mouse was allowed to explore the entire social test box for a 5-minute session. The test was videotaped and the time spent in each chamber of the apparatus during the two 5-minute sessions was measured (Moy et al., 2004). The first session controlled for the place preference. No significant difference between groups was observed during this period; the second session allowed the assessment of the sociability.

3.6 Barnes maze

This model is based on aversion to open and lighted spaces, which motivates the rodent to seek shelter and assesses the spatial learning capability of rodent. The Barnes maze consisted of a circular surface (90 cm diameter, 206 cm^2) raised 80 cm from the floor with 20 circular holes around its circumference. The table surface was brightly lit by overhead lighting. Visual cues (colored

ACCEPTED MANUSCRIPT

shapes) were placed around the table in plain sight of the animal. A black Plexiglas box was placed underneath one of the holes as an escape chamber (Suppl Fig 3A). Two 5-min sessions of training were performed per day for 4 consecutive days and videotaped. The mouse was placed on the middle of the device and the latency for entering the escape box (or at least two paws in the box for > 2 sec) was scored to establish a learning curve during 4 consecutive days. On days 5 and 9, probe trials were conducted without the escape box; time spent in each quadrant, a virtual space around each hole (8.2 cm^2) was recorded over 90 sec. Neither the distance traveled nor the mean speed was significantly different between SE and EE-housed mice.

3.7 Statistical analysis

Comparisons between two conditions were made using the nonparametric Kruskal and Wallis test followed by the Dunn's post-hoc test except for paired data (i.e. Fig. 1G, Barnes maze), which was analyzed using the Friedmann test. Data are presented as means ± SEM. Statistical significance was set at *p <0.05 and **p <0.01, ***p <0.001.

4 - Hippocampal neurogenesis

We measured hippocampal neurogenesis in EE and control SE mice using intra-peritoneal (*ip.*) injections of bromodeoxyuridine (BrdU) (50 mg/kg, once a day for 5 consecutive days) followed by immunohistochemistry quantification of BrdU-stained cells in the hippocampus, according to (Heurteaux et al., 2006). Briefly, mice were euthanized with pentobarbital 24 hours or 21 days after the last injection, perfused with ice-cold HBSS (pH 7.4, 1 mg/mL EDTA) and fixed by 3.2% paraformaldehyde (PFA) through intra-cardiac perfusion. The brain was rapidly removed and fixed in 3.2% PFA for 48h. 40 μm thick serial sections of PFA-fixed brains were cut through the hippocampus on a vibratome (Microm). One slice out of every six was collected for a total number between eight and twelve sections to proceed to immunohistochemistry staining using a monoclonal

ACCEPTED MANUSCRIPT

mouse anti-BrdU (1:7000; BD Biosciences). For BrdU chromogenic immunodetection, sections were incubated for 1 hour in biotin-conjugated species-specific secondary antibodies (1:400, Vector Laboratories), followed by a peroxidase-avidin complex solution according to the manufacturer's protocol. The peroxidase activity of immune complexes was visualized with 3,3′-diaminobenzidine (DAB) staining using VectaStain ABC kit (Vector Laboratories). BrdU-labeled cells of granular and subgranular layers were counted in each section under a light microscope. The total number of $BrdU^+$ cells counted per eight slices was multiplied by 6 to obtain the total number of $BrdU^+$ cells per DG.

We also performed a double labeling experiment with both the monoclonal mouse anti-BrdU (1:500; BD Biosciences) and a secondary donkey anti-mouse Alexafluor 488 (Invitrogen), and the polyclonal rabbit anti-NeuN (1:1000, Abcam Ab177487) antibody coupled to a secondary donkey anti-rabbit Alexafluor 594 antibodies (Invitrogen) to investigate which of the new cells were differentiated into neurons, following the protocol (Wojtowicz and Kee, 2006).

5. Spinogenesis

Mice were deeply anesthetized with pentobarbital and perfused with 3.2 % paraformaldehyde (PFA). A single brain serial section (200 µm) was cut at the level of the hippocampus on a vibratome (Microm) from the same mice as those used for the neurogenesis experiments approximately between bregma 2.30 and 2.50 mm. The slices were then stored in 0.1 % (wt/vol) NaN_3 in PBS at 4°C until microinjections of the fluorescent dye Alexa Fluor 568 (ThermoFisher Scientific) by iontophoresis coupled with pressure ejection using micropipettes with high tip resistance (15-20 MΩ). The slices were then mounted using a Vecta-Shield mounting medium and imaged within a few days.

Stacks of images from segments of 45 µm long dendrites were obtained through a 63X/1.4 NA objective on an LSM780 laser-scanning confocal microscope (Carl Zeiss, Le Pecq, France). A

ACCEPTED MANUSCRIPT

detailed morphometric analysis of the spines was first performed using an in-house macro-program from ImageJ software (Rasband, W.S., ImageJ, US National Institutes of Health, Bethesda, Maryland, USA, http://imagej.nih.gov/ij/, 1997-2012). Briefly, after a maximal projection of the images of each stack and segmentation to produce a binary image (Suppl Fig 5), the skeleton of the dendritic tree was analyzed and its length measured. The number of intersections and spines were determined and after binary thinning the length of the principal axis was measured. These images were subsequently analyzed with NeuronStudio software and spines were classified into "thin", "mushroom" and "stubby" according to (Peters and Kaiserman-Abramof, 1970) using the following parameters: the maximum and minimum spine heights were set at 3.5 and 0.5 µm, respectively. Minimum stubby spine was set at 22 voxels. In each group, we used 1874-2856 segments of dendrites from 82-106 neurons from 4-6 mice.

6. Electrophysiology

6.1 Acute brain slices

Mice were deeply anesthetized with halothane, then decapitated and brains were immediately placed in ice-cold gassed medium (95% O2/5% CO2) containing (in mM): 125 NaCl, 2.5 KCl, 1 $MgCl_2$, 0.4 $CaCl_2$, 1.25 NaH_2PO_4, 26 $NaHCO_3$ and 25 glucose. Coronal slices of hippocampus (350 µM thick) were cut with an HM650V vibratome (Microm, Walldorf, Germany) and placed in a holding chamber at 34 °C for 1 h. Slices were then transferred into a phosphate bicarbonate buffered saline (PBBS) composed of (in mM): 125 NaCl, 2.5 KCl, 1 $MgCl_2$, 2 $CaCl_2$, 1.25 NaH_2P0_4, 26 $NaHC0_3$ and 25 glucose, pH 7.4 when bubbled with 95% O_2 and 5% CO_2.

The same mice were used both for patch-clamp and LTP experiments using two different electrophysiology setups simultaneously.

6.2 Patch clamp

ACCEPTED MANUSCRIPT

CA1 pyramidal neurons were patch-clamped in the whole-cell configuration. This technique allows for the recording of currents from the whole surface of a single neuron in the living slice while it is still connected with the rest of the neuronal network. Using pipettes (2-8 MΩ) filled with a cesium chloride (CsCl) solution supplemented with N-(2,6-dimethylphenylcarbamoylmethy-l)triethylammonium bromide (QX314, a sodium channel blocker to block action potentials) we recorded the glutamatergic excitatory post-synaptic currents (EPSCs) which were pharmacologically isolated using the $GABA_A$ receptor antagonist bicuculline (10 µM) in the bath solution. We recorded both spontaneous (without the sodium channel inhibitor tetrodotoxin, TTX) and miniature (in the presence of 2 µM TTX) EPSCs. Three minute recordings were used to determine the properties of the spontaneous events. 3-16 neurons were recorded in 2-5 mice for each group.

6.3 Long-term potentiation (LTP)

Hippocampal slices were placed under a Nomarski microscope (Zeiss, Germany) equipped with an infrared video camera (Axiocam, Zeiss) in a recording chamber superfused at a flow rate of 1 $mL.min^{-1}$ with oxygenated PBBS. Pictures were taken using a digital camera (Axiocam, Zeiss) connected to image-acquisition software (Axiovision, Zeiss). Recordings were made at room temperature (20-25°C) using an Axopatch 200B (Axon Instruments, Foster City, CA, USA) connected via an interface (Digidata 3200) to a computer running pClamp (Axon Instruments). At the beginning of each recording, a tungsten bipolar stimulating electrode was positioned at the stratum radiatum for stimulation of the Schaffer collateral projections to CA1, using a stimulator (STG4002 Multichannel systems) connected to the computer. Field potentials in the dendritic tree of CA1 neurons were recorded with pipettes (made from borosilicate glass capillary (Hilgenberg, Masfeld, Germany) with resistance of 3-6 MΩ when filled with extracellular solution). The intensity of stimulation was adjusted in each experiment to evoke about 50% of the maximal field potential amplitude without appreciable population spike contamination. Low-frequency stimulation (0.1 Hz) was applied to the Schaffer collaterals to establish a stable baseline (for 20-30 min) of the excitatory

ACCEPTED MANUSCRIPT

post synaptic potential (EPSP) slope, after which LTP was induced by high-frequency stimulation (HFS; 100 Hz/1 sec), followed by the initial low frequency stimulation. To analyze the time course of the EPSP slope, the recorded fEPSP data were routinely averaged over 1 min (n=6). Successful induction of LTP was obtained when the post-HFS EPSP exceeded that seen before HFS and was maintained for at least 40-60 min. 5-6 mice were used per group.

6.4 Drugs and reagents

APV ((2R)-amino-5-phosphonovaleric acid, a N-methyl-D-aspartate (NMDA) receptor antagonist) and 6-cyano-7-nitroquinoxaline-2,3-dione (CNQX), α-amino-3-hydroxy-5-methyl-4-isoxazolepropionic acid receptor (AMPA)/Kainate receptor antagonist, QX314, TTX and bicuculline were from Sigma Aldrich, France.

6.5 Data analysis

Voltage clamp data were digitized at 0.5 kHz using a Digidata interface coupled to a microcomputer running p-Clamp 9 (Axon Instruments). Currents were digitally filtered at 1–3 kHz. Average data were expressed as mean ± SEM, n=number of neurons that were recorded. Statistical significance between groups was calculated using the Student t-test, the ANOVA followed by the Fisher test, or the Kruskal-Wallis followed by the Dunn's test and were considered significant at * $p < 0.05$, ** $p < 0.01$ and *** $p < 0.001$ using a statistical software package (SigmaStat 2.03, Jandel Sci and Graph Prism software). Cumulative histograms were compared by Kolmogorov-Smirnov analysis using Clampfit (Axon Instruments), with an equal number of events for each group. Significant differences between two groups of data were determined using a Mann-Whitney test for non-parametric data.

7- RNA isolation and quantitative polymerase chain reaction (qPCR)

Total RNA from hippocampus tissue (entire, or dissections from DG and CA from the same mice) were isolated using the Trizol® RNA extraction kit (Invitrogen) according to the

ACCEPTED MANUSCRIPT

manufacturer's recommendations, followed by a RQ1 DNAse (Promega) treatment. First-strand cDNAs were synthesized from 2 µg of total RNA with 200 U of SuperScript III reverse transcriptase (SuperScriptIII, Invitrogen) in the appropriate buffer in the presence of 25 µg/mL random primers, 0.5 mM desoxyribonucleotide triphosphate mix, 5 mM dithiothreitol, 40 U RNAsin (Promega). The reaction was incubated for 5 min at 25 °C, 50 min at 50 °C, then inactivated 15 min at 70 °C. Quantitative PCR was performed using the SYBRgreen method (Roche) with the LightCycler 480 sequence detector system (Roche Diagnostics). ß-actin and GAPDH were used as housekeeping genes for normalization. Primers were purchased from QIAGEN (QuantiTect primer assay, QIAGEN). The following primers were used:

Gene	**Cat. No.**	**Gene**	**Cat. No.**
ß-actin	QT01136772	Slc17a7	QT00148841
Bdnf	QT00097118	Syn1	QT00171206
Cntf	QT00303478	Syn2	QT00152698
Cx3cr1	QT00259126	Syp	QT01042314
Dlg4	QT00121695	Syt1	QT00167300
Homer1	QT00129983	**DG and CA genes**	
Icam1	QT00155078	Dsp	QT00321496
Igf1	QT00121695	Tdo2	QT00150409
Ntf3	QT02524942	Tyro3	QT00197659
Ntf5	QT00254058	Meis1	QT00172557

To confirm that the dissected tissue is DG we measured specific gene expression (Dsp, Tdo2 and Ammon's horn enriched genes, Tyro3, Meis1) using quantitative Polymerase Chain Reaction (qPCR) according to (Hagihara et al., 2009). Gene expression was analyzed following the ΔΔCt method.

Statistical analysis: for each gene, we first performed a non-parametric Kruskal-Wallis test on ΔCt values followed by exact two-sample Fisher-Pitman permutation tests comparing SE to EE at 3W and 4W, and in each group (SE or EE) comparing 3W to 1W and 4W to 1W (or 3W to 2W and 4W

ACCEPTED MANUSCRIPT

to 2W for Ab-injected mice). The obtained *p* values were corrected using the FDR method of Benjamini-Hochberg for a total of 8 comparisons per gene.

8- T cell immunostaining in choroid plexus

Mice were deeply anesthetized with pentobarbital and transcardially perfused with ice-cold HBSS. Choroid plexus from individual mice were collected rapidly in cold PBS and fixed on slide in a 2.5 % PFA solution. For this experiment, we used the same mice as the ones used for hippocampus qPCRs. Choroid plexus cells were stained with monoclonal mouse anti-actin (1:300, Abcam Ab8227) and a secondary goat anti-mouse Alexafluor 488 (1:1000, Invitrogen) and the polyclonal hamster anti-CD3 (1:200, Abcam Ab5690) antibody coupled to a secondary goat anti-hamster Alexa fluor 594 antibodies (1:1000, Invitrogen) to localize T cells in the choroid plexus.

9- Immune cell staining, flow cytometry and cell sorting

Staining of brain immune cell surface antigens was performed as previously described (Cazareth et al., 2014). Briefly, Fc receptors were blocked with a purified rat anti-mouse CD16/CD32 (2.4G2, Fc block) antibody (BD Biosciences). Cells were incubated with the appropriate combination of conjugated antibodies: anti-CD11b-PerCP-Cy5.5, anti-CD45-APC-Cy7, anti-CD3-FITC, anti-CD8-PE-Cy7 or anti-CD8-PE, anti-CD4-BV510 or anti-CD4-PB, anti-CD44-PE and anti-CD62L-A700 (BD Biosciences) antibody for 30 min. Phenotype analysis cells were performed in a flow cytometer (LSR II Fortessa, BD). Immune cells were sorted on a Becton-Dickinson FACS Aria III.

10 - $CD8^+$ T cell enrichment from splenocytes

ACCEPTED MANUSCRIPT

A single cell suspension from spleen was obtained by mashing the organs through nylon sieves in RPMI 1640 (Gibco, Life Technologies). Erythrocytes were eliminated by treatment with ammonium chloride potassium (ACK). Splenic $CD8^+$ T cells were enriched to a purity of > 96% by negative selection with the EasyStep mouse $CD8^+$ T cells enrichment kit (StemCell Technologies).

11- Immune cells isolation from adult brain

Mice were deeply anesthetized with a lethal injection of pentobarbital. Immune brain cells were isolated from whole-brain homogenates using a protocol adapted from Cardona et al. (Cardona et al., 2006) as previously described in (Cazareth et al., 2014). Mice were transcardially perfused with ice-cold HBSS containing 1 mg/ml EDTA. Brains were collected and homogenized in PBS, resuspended in PBS containing 3mg/ml collagenase D (Roche Diagnostics) and incubated 20 minutes at 37°C. After incubation, brain homogenates were filtered on 70 µm pore size cell strainers (BD Biosciences), centrifuged (10 min, 2000 rpm), washed and resuspended in 6 ml of 38% isotonic Percoll (GE Healthcare), before centrifugation (20 min, 2000 rpm, 4°C). The surface ring containing myelin and debris was discarded. Cell pellets containing brain immune cells were collected washed with PBS containing 0.5% BSA and 2.5mM EDTA and labeled for subsequent cell sorting and/or flow cytometry analysis.

12- RNA Sequencing

12.1 Cell sorting

Mice were deeply anesthetized with a lethal injection of pentobarbital and transcardially perfused with ice-cold HBSS containing 1 mg/mL EDTA. Choroid plexus and spleen were collected in two independent series of experiments. Splenocytes were suspended by mechanic dissociation and immune cells were prepared after ACK treatment to remove red blood cells. Choroid plexus were homogenized in PBS containing 3mg/mL collagenase D (Roche Diagnostics) and incubated for 20

ACCEPTED MANUSCRIPT

minutes at 37°C. Cell pellets containing choroid plexus immune cells were collected, washed with PBS containing 0.5% BSA and 2.5mM EDTA and labeled. Staining of immune cell surface antigens from choroid plexus and spleen was performed as previously described (Cazareth et al., 2014). Immune cells were identified according to the labeling of anti-CD45, anti-CD11b, anti-CD3, anti-CD4 and anti-CD8 conjugated antibodies (BD Biosciences). $CD45^+$ $CD11b^-$ $CD3^+$ $CD4^+$ and $CD45^+$ $CD11b^-$ $CD3^+$ $CD8^+$ cells were sorted by the FACSAria cell sorter (BD Biosciences)

12.2 cDNA preparation

Cells were directly collected into 0.2 mL tube stripes in a lysis reaction with a final volume of 13.5 ul according to Arguel *et al.*, all incubations steps occurred in a Veriti thermal cycler (Applied Biosystem). Reverse transcription (RT) mix was added during incubation at 10°C immediately following lysis, tubes were vortexed and centrifuged briefly and put back in thermocycler for RT incubations steps. Template switching oligonucleotide (TSO) was designed as per Picelli et al. (Picelli et al., 2014), with a LNA on 3 prime extremity 5'-GCA ATG AAG TCG CAG GGT TGN NNN HHH HrGrG lnG-3'.

For $CD8^+$ T cells from the choroid plexus, the number of cells varied from 2 to 20 cells per sample, thus the entire RT volume was added to the PCR amplification reaction, leading to 31.5µl of RT in a final volume of 83µl, 60µM barcode primer, 0.6µM biotinylated PCR primer. For spleen, 1000 cells per sample were used, and after RT, 1/10 of cDNA was used for sequencing.

12.3 Library preparation

All 48 barcoded cDNAs were pooled and 20 nanograms was used as template for Ion Proton sequencer tagmentation protocol as described previously (Arguel et al., 2017).

12.4 Sequencing

ACCEPTED MANUSCRIPT

Libraries were sequenced on a Proton Ion PI™ Chip V3 (Thermo), generating 38M reads for the choroid plexus and 170M for the spleen experiment. Single end reads were then processed with a custom analysis pipeline. The first step was to remove the 3p adaptor "CTGTCTCTTATACACATCT" and the sequenced front adaptor: "AAGTCGCAGGGTTG" using Cutadapt (v1.2.1). Immediately after the front adaptor we stipulated an 8 base pattern requirement in accordance with the design UMI N4H4 (N=ATCG, H=ATC only) followed by a stretch of GGG. Reads without those specifications were discarded from further analysis to avoid artefactual molecules that were produced by the creation of new UMI sequences related to sequencing errors, especially indels that are frequent in Ion Torrent reads. Reads with a template sequence length of under 50 bases were discarded. This filtration process removed 32% and 34% of the total number of reads for the plexus and the spleen experiment respectively. Mapping of the identified cDNAs was conducted with the STAR_2.4.0a versus mm10 mouse genome build using RNAseq Encode recommendations. For molecule counting based on UMI counts, we used the Dropseq Core Computational Protocol version 1.0.1 (dropseq.jar) from McCarrol (Macosko et al., 2015) using the GTF gene model from Ensembl release GRCm38.83. Digital Expression function of dropseq.jar was called with default parameters (edit distance=1) to produce a matrix of molecule counts which was used in subsequent statistical analysis.

12.5 Statistical analysis and biological theme analysis

Choroid plexus and spleen samples were analyzed separately. Quality control of RNAseq data was performed with in-house R scripts. The purity of biological samples was verified by inspection of Cd4, Cd8a and Cd8b1 expression levels. CD4 (CD8 respectively) samples with non-zero expression levels for Cd8a or Cd8b1 (Cd4 respectively) were considered of poor quality and excluded. Low abundance genes were filtered out, then sequencing depth normalization and differential expression analysis was carried out using the Bioconductor package DESeq2 (Love et al.,

ACCEPTED MANUSCRIPT

2014). P-values were adjusted for multiple testing using the Benjamini-Hochberg procedure, which controls the false discovery rate. No gene reached statistical significance at the 0.05 level after adjustment. For choroid plexus samples, mild differential expression was observed between the enriched and standard environment and candidate differentially expressed genes were selected based on a nominal $p < 0.05$. For spleen samples, differentially expressed candidate genes were selected based on a combination of nominal $p < 0.05$, absolute log2 fold-change >1 and an average log2 expression level > 2. Heatmaps were generated using the R package pheatmap (Pretty Heatmaps V 1.0.8, https://CRAN.R-project.org/package=pheatmap).

Canonical pathways and molecular function analyses were carried out using Ingenuity Pathway Analysis (IPA, Qiagen Bioinformatics). Gene Set Enrichment Analysis was performed using GSEA, by comparing the modifications observed in EE vs SE to modifications observed in the same subcellular population in the immune set of data (C7) or a larger ser of data (C2). Pathways with a normalized $p < 0.05$ were considered to be enriched.

13 -T cell proliferation and cytokine production

For T cell stimulation, 96-well microplates were coated with 10 µg/mL of anti-CD3 mAb in sterile PBS and incubated overnight at 4°C. One day later, wells were washed three times with sterile PBS to remove non-bound soluble antibody. 3.10^5 enriched $CD8^+$ T cells from spleen and 2 µg/mL of soluble CD28 antibody was added in a classic culture medium and incubated 72 hours at 37°C, 5% CO_2. Two independent experiments were performed (one for sorting, and the other for negative selection). A third independent sorting experiment was performed where CD8+ T cells were submitted to 4h of stimulation with phorbol myristate acetate (PMA, 20 ng/ml) / ionomycin (1 µg/ml) in a classic culture medium (PMA/Iono). IFNγ and TNFα levels were measured by MSD (Meso Scale Discovery) following the manufacturer's recommendations.

ACCEPTED MANUSCRIPT

For assessing T cell proliferation, $1x10^6$ $CD8^+$ T cells were cultured with 5 µM CFSE in 48 wheels plate with different concentrations (6, 13 and 25 µg/mL) of anti-CD3 and 2 µg/mL of soluble anti-CD28. After 72h, cells were stained and acquired by cytometry (Fotessa, BD). We used CFSE labeling of $CD8^+$ T cells to measure proliferation. The dye is long lasting and well-retained within labeled cells.

14- Astrocytes and microglia isolation from adult brain

Mice were euthanized with pentobarbital, perfused with ice-cold HBSS (pH 7.4, 1 mg/mL EDTA) through intra-cardiac perfusion. Hippocampi were dissected and astrocytes and microglia were sorted out using sequential labeling with anti-ACSA2 and anti-CD11b magnetic microbeads, respectively. Briefly, single-cell suspensions from hippocampi were obtained after use of Adult Brain Dissociation Kit (Miltenyi Biotec) in combination with the gentleMACS Dissociator (Miltenyi Biotec). Fc receptors were blocked with FcR Blocking Reagent (Miltenyi Biotec). Then, the ACSA-2^+ cells were magnetically labeled with anti-ACSA-2 microbeads (Miltenyi Biotec). The cell suspension was loaded onto MACS® Column (Miltenyi Biotec), which was placed in the magnetic field of MACS Separator (Miltenyi Biotec). The magnetically labeled ACSA-2^+ cells were retained within the column. The unlabeled cells running through this cell fraction was used to label and sort $CD11b^+$ cells by using the same protocol as ACSA-2^+ cells isolation.

ACCEPTED MANUSCRIPT

RESULTS

1. EE-induced behavior changes are dependent on $CD8^+$ T cells

We first confirmed that $CD8^+$ T cell depletion did not impact the animal weight (Suppl Fig 1 D) or locomotion as assessed in the Rotarod test (Fig 1A).

$CD8^+$ T cell depletion abolished the effects of EE on anxiety, as measured by multiple behavior tests including the open-field test (Fig 1B), the light/dark test (Fig 1C), and the novelty suppressed feeding test (Fig 1D). In contrast, $CD8^+$ T cell depletion did not alter the beneficial effects of EE in the forced swimming test (Fig 1E) and the social interaction test (Fig 1F).

In a second set of experiments, the Barnes maze test was performed to assess the role of $CD8^+$ T cells in spatial learning (Suppl Fig 3). Although EE mice found the hole faster than SE mice on the first day of training, the performances of all groups of mice were similar at the end of the training period (Fig 1G) and on the first test day (day 5, Fig 1H left and Supp Fig 3B), suggesting that neither the EE nor the $CD8^+$ T cell depletion was involved in short-term memory. On day 9 (Fig 1H, right and Suppl Fig 3C), EE mice injected with the control antibody spent significantly more time in the vicinity of the target hole compared to control SE mice whereas $CD8^+$ T cell depletion abolished the EE-induced increase in time spent around the target hole.

In conclusion, of the tests we carried out, the behavioral tests of anxiety and spatial learning involving hippocampus function, such as the Barnes maze, were affected by $CD8^+$ T cell depletion.

2. EE-induced hippocampal plasticity is dependent on $CD8^+$ T cells

2.1 EE-induced neurogenesis is $CD8^+$ T cell dependent

EE increases hippocampal thickness, dendritic arborization and cell number (Kempermann et al., 1997). We first investigated whether $CD8^+$ T cell depletion affected EE-induced changes in the number of cells, dendrites, or spines. In mice injected with a control antibody, EE housing increased

ACCEPTED MANUSCRIPT

neurogenesis as illustrated by the increase in $BrdU^+$ cells in DG (Fig 2A). This effect was observed by counting the number of $BrdU^+$ cells 24 hours (Fig 2Aa) and 21 days after BrdU injection (Fig 2Ab) further demonstrating that EE promoted both cellular proliferation and survival, respectively. Depletion of $CD8^+$ T cells partially abolished the EE-induced increase in the number of $BrdU^+$ cells (Fig 2A, 2B). Therefore, the EE-induced increase in DG cell proliferation and survival is at least partially $CD8^+$ T cell dependent.

Because BrdU could be incorporated into both neuronal and glial cells, BrdU/NeuN co-staining was performed to assess the specific BrdU incorporation into neurons (Fig2B). Regardless of the housing conditions or Ab treatments, no significant difference was observed between the number of double (BrdU/NeuN) and single (BrdU) positive cells, indicating that in our conditions, the BrdU incorporation occurred almost exclusively in neuronal populations.

We subsequently investigated whether the effect of $CD8^+$ T cells was antigen-dependent. We used OT-I mice in which all T cells react to an ovalbumin (OVA)-derived peptide bound to $H2\text{-}K^b$ MHC class I molecules. Neurogenesis in the DG hippocampus was increased in OT-I mice housed in EE compared to those housed in SE (Fig 2Ac). This suggests that the impact of $CD8^+$ T cells on EE-induced neurogenesis was antigen-independent.

Because neurogenesis is regulated by neurotrophic factors, the expression level of several neurotrophic factors was measured in DG using qPCR over the time of housing in SE and EE. In mice raised in SE, the expression of neurotrophic factor genes was relatively stable over time from 1 week housing for Igf1 and Ntf3, reaching significance only at 4 weeks for Ntf5 and Cntf, and at 3 weeks for Bdnf with a two-fold increase only. By contrast, in EE mice, the expression of Bdnf, Cntf, Igf1, Ntf3 and Ntf5 progressively increased, reaching statistical significance after 3 weeks for Bdnf, Igf1, Ntf5 and Cntf and increasing significantly more than in SE mice for Bdnf and Igf1 at 3W (Fig 3A). In order to evaluate the effect of $CD8^+$ T cell depletion, the expression of neurotrophic factor genes was assessed over the time between 2 and 4 weeks of EE housing. For mice treated with

ACCEPTED MANUSCRIPT

control Ab, EE induced a significant increase of the expression of Bdnf and Ntf3 that was abolished by $CD8^+$ T cell depletion. This suggests that $CD8^+$ T cells played a critical role in neurogenesis process (Fig 3B).

2.2 EE-induced synaptogenesis in CA1 is dependent on $CD8^+$ T cells

We next investigated the role of $CD8^+$ T cell depletion on the number and type of basilar dendrite spines in pyramidal CA1 neurons using a previously described method (Suppl. Fig 4 A, B). Spine density (Fig 4A), head diameter (Fig 4B) and length (Fig 4D) were increased in EE mice compared to SE mice. The ratio between the number of thin and stubby spines was also different between SE and EE mice (Suppl Fig 4C and D). These differences were partially abolished by $CD8^+$ T cell depletion, although head diameter (Fig 4B) and spine length (Fig 4D) attenuation was mainly due to an increase following $CD8^+$ T cell depletion in SE. Altogether, these results demonstrate that EE-induced spinogenesis in pyramidal CA1 neurons of the hippocampus was dependent on $CD8^+$ T cells, although $CD8^+$ T cell depletion also affected spine shape in SE conditions.

EE-induced changes in spine morphology were expected to be associated with altered expression of genes encoding synaptic proteins such as the neurotrophic factor Bdnf, presynaptic proteins (synapsin 1, synapsin 2, synaptophysin and synaptotagmin) and proteins expressed at the glutamatergic synapse (Dlg4, homer1, Slc17a7). To investigate this further, gene expression was measured by RT-qPCR from CA of SE and EE mice as a function of housing time (Figure 5A). The level of several mRNAs increased over time in EE mice, reaching statistical significance at 3 weeks for Bdnf, Syt1, Syn1, Syn2, Syp, Homer1 and Slc17a7. By contrast, in SE, only Bdnf and Syn2 mRNAs levels increased at a housing time of 4W, suggesting that EE promoted the expression of these genes involved in synaptogenesis over time. These differences were abolished upon depletion of $CD8^+$ T cells (Figure 5B) therefore demonstrating a critical role for these cells in this phenomenon.

ACCEPTED MANUSCRIPT

2.3 Effects of $CD8^+$ T cell depletion on glutamatergic transmission at the CA1 synapses

We then sought to further characterize the effects of $CD8^+$ T cell depletion on spontaneous glutamatergic activity in SE and EE mice (Fig 6). Thus, we used a patch-clamp technique to record both spontaneous EPSCs (sEPSCs, in the presence of 10 µM bicuculline to block $GABA_A$ IPSCs) and miniature EPSCs (mEPSCs, in the presence of bicuculline + 2 µM TTX to block the action potentials) on CA1 pyramidal neurons. In control conditions, EE mice exhibited a 1.5-2 fold increased frequency of both sEPSCs and mEPSCs compared to SE mice, suggesting an increased number of synaptic release sites (Fig 6 and Suppl. Fig 5), which correlated with an increase in the number of spines counted in brain slices at the level of the basal secondary dendrites of CA1 neurons, as previously shown (Hosseiny et al., 2015). The amplitude and the time constant of decay of the events were unaffected in mice injected with control antibodies. The EE-induced increase in sEPSC frequency was no longer observed in $CD8^+$ T cell depleted mice, but $CD8^+$ T cell depletion caused a significant increase in sEPSC frequency in SE (Fig 6A), whereas no effect on amplitude or time constant of decay was observed between these groups. When considering the mEPSCs, however, no proper effect of $CD8^+$ T cell depletion was observed on their frequencies in SE mice whereas the EE-induced increase in mEPSC frequency was abolished.

2.4 Effect of $CD8^+$ T cell depletion on LTP

LTP was reduced in EE mice as compared to SE mice injected with control antibodies (Fig 6B and C). This effect was abolished by $CD8^+$ T cell depletion (Fig 6C).

Overall our results demonstrated that EE-induced neurogenesis and increased synaptic activity were dependent on $CD8^+$ T cells.

3. $CD8^+$ T cells are phenotypically different in SE and EE mice

3.1 $CD8^+$ T cell number and function

ACCEPTED MANUSCRIPT

SE and EE mice exhibited a similar number of $CD8^+$ T cells in spleen tissue, as well as similar CD8/CD4 ratios in spleen (Suppl Fig 10A). We investigated whether $CD8^+$ T cells from SE and EE mice differed in their ability to secrete cytokines or proliferate in response to *in vitro* stimulations with an anti-CD3/CD28 Ab or with the TCR independent PMA/Iono stimulation. $CD8^+$ T cells from EE mice secreted increased levels of TNFα but similar levels of IFNγ, as compared to cells from SE mouse spleen (Fig 7A, B, C). Compared to those from SE mice, $CD8^+$ T cells from EE mice demonstrated increased proliferation as assessed by CFSE dilution and flow cytometry (Fig 7D, E). In contrast, $CD4^+$ T cells from SE and EE mice did not differ in their ability to secrete TNFα or IFNγ after stimulation, or to proliferate (Suppl Fig 6A, B).

3.2 Splenic $CD8^+$ T cells from SE and EE mice exhibit different transcriptomic profiles

Transcriptomic profiles were compared between $CD8^+$ T cells of SE or EE mice. To this end, we purified $CD8^+$ T cells from the spleen of SE and EE mice by flow cytometry (1000 cells / mouse, n = 6 / group) and analyzed these cells by RNA sequencing transcriptomic analysis. As expected, Cd8a and Cd8b1, but not Cd4 mRNAs were detected in all samples (Supp Fig 7A). Among 4856 transcripts, 208 and 225 mRNAs were differentially expressed in SE and EE mice (Log_2 FC > 0.5 or < 0.5, $p < 0.05$) (Fig 8). Ingenuity Pathway Analysis (IPA) with the following parameters: $p < 0.05$, Log_2 FC 0.5 and intensity 10, revealed that differentially expressed genes that were enriched in several signaling pathways, including the estrogen receptor, glucocorticoid signaling and TNF-R1 and TNF-R-2 signaling pathways (Suppl Fig 8). We also used a Gen Set Enrichment Analysis (GSEA, Broad Institute) to assess the overall differences between EE and SE conditions in $CD8^+$ T cells from spleen compared to an immunology data set that was previously published by others (named C7). We selected the pathways that corresponded to the variations observed in EE vs SE with a $p < 0.05$ and ordered them according to the normalized enrichment score and considered only those experiments that concerned $CD8^+$ T cells (Suppl Fig 9). Variations in expression between the sets of genes obtained from SE to EE were similar to variations in expression observed in naïve vs.

ACCEPTED MANUSCRIPT

memory or in effector vs. naive $CD8^+$ T cells. Compared to a more general set of GSEA data (named C2) and focusing on the reactome pathways closest to the set of genes that differed between EE and SE, we also found similarities with the TGF-β receptor signaling reactome.

As a conclusion, splenic $CD8^+$ T cells of mice raised in EE vs. SE differ in the expression of a set of genes, in agreement with differences in previously described cell profiles.

3.3 $CD8^+$ T cells from the whole brain

3.3.1 $CD8^+$ T cells are present in the whole brain (i.e. including blood vessels, meninges, CSF, and the choroid plexus)

As previously published, a small number of $CD3^+$ T cells were detected in the whole brain (445.9 ± 79.7, n=11). Of note, $CD8^+$ T cells accounted for 30% and 50% of $CD3^+$ T cells in spleen and whole brain respectively (Suppl Fig 10A). Among $CD8^+$ T cells detected in the whole brain, about 50% (216.8 ± 30.7, n = 11) were present in the choroid plexus. Immunostaining showed that they were close to epithelial cells (Suppl Fig 10B).

3.3.2 Choroid plexus $CD8^+$ T cells transcriptomic signature is different in SE and EE

RNAseq experiments were performed on isolated $CD8^+$ and $CD4^+$ T cells from the choroid plexus of SE and EE mice (10 cells / mice, 12 mice / group) and the transcriptomic profiles were analysed by single cell RNAseq methods. As expected, Cd8a and Cd8b1, but not Cd4 mRNAs were found in $CD8^+$ T cells. In contrast, Cd4 but neither Cd8a nor Cd8b1 mRNAs were found in $CD4^+$ T cells (Suppl Fig 7B). In $CD8^+$ T cells, among 2851 transcripts, 20 genes were upregulated and 20 genes were downregulated between SE and EE mice (p value < 0.05; log2FC > 0.5 or <-0.5). Among them, Lat and Lck (pathway activated by the TCR) and Il17r decreased in EE.

Several genes whose expression varied in EE vs. SE in $CD8^+$ T cells from choroid plexus such as Lat, Lck and Tagln2 were characteristic of lymphocytes (Fig 9).

ACCEPTED MANUSCRIPT

To determine the pathways that were involved in the differences between whole brain $CD8^+$ T cells from EE and SE mice, we performed an IPA with the following parameters: $p < 0.05$, Log_2 FC 0.5 and intensity 10 (Suppl Fig 8). This analysis revealed that differentially-expressed genes were enriched in several signaling pathways including T-cell receptor and IL17-A signaling pathways.

As for splenic CD8+ T cells, we used GSEA to analyze the overall changes between EE and SE conditions in $CD8^+$ T cells from choroid plexus compared to data previously published by others in the immunology set (C7). We selected the pathways that corresponded to the variations observed in EE vs SE with a $p < 0.05$ and ordered them according to the normalized enrichment score. We selected only the experiments which were conducted using the same cellular type (i.e. $CD8^+$ T cell; Suppl Fig 9). Variations in the expression of the gene sets obtained from SE to EE were closer to variations in expression observed in naïve vs. memory or in effector vs. naive $CD8^+$ T cells.

In conclusion, the housing conditions induced changes in the expression profile of $CD8^+$ T cells in both the periphery and at the choroid plexus. The relative differences between EE and SE expression sets could indicate a favored "memory" profile of $CD8^+$ T cells in EE.

3.3.3 Brain repartition of SE and EE $CD8^+$ memory T cells compared to the spleen

CD44 is an indicative marker for memory T cells, expressed at the membrane of $CD8^+$ T cells. We decided to compare, both in the whole brain and the spleen, the repartition among $CD8^+$ $CD44^+$ T cells between cells expressing a high and a low level of CD62L (respectively referred to as "central memory T cells" and "effector memory T cells" (Tough, 2003); Fig 10A, B).

The percentage of $CD62L^{low}$ and $CD62L^{hi}$ among the $CD8^+$ $CD44^+$ T cell population differed in the whole brain between in EE and SE: the percentage of $CD62L^{low}$ cells significantly increased (Fig 10C) while the percentage of $CD62L^{hi}$ cells significantly decreased (Fig 10D). Conversely, the percentage of $CD62L^{hi}$ and $CD62L^{low}$ cells in spleen showed no significant modifications in SE and

ACCEPTED MANUSCRIPT

EE (Fig 10C, D). In contrast, no variation among $CD4^+$ T cells populations from whole brain and spleen was observed (Suppl. Fig 6 C).

In conclusion, $CD8^+$ T cells from EE mice are different compared to SE mice, both in the periphery and the choroid plexus. Furthermore, profiles of peripheral $CD8^+$ T cells and whole brain $CD8^+$ T cells located at the choroid plexus also differed.

4. In mice raised in EE, hippocampal astrocytic growth factor gene expression is dependent on $CD8^+$ T cells.

To determine whether glial cells (astrocytes or microglia) could serve as intermediates between $CD8^+$ T cells and hippocampus to allow the changes in plasticity induced by EE, we sorted sequentially astrocytes and microglia out from hippocampi of mice raised in SE or EE and depleted or not from $CD8^+$ T cells.

We validated our sorting protocol by measuring with RT-qPCR the expression level of the specific microglial Cx3cr1 gene, which was significantly higher in microglia relative to astrocytes (Suppl Fig 11 A).

Expression levels of the trophic factor genes Bdnf, Igf1 and NTF5 were determined by RT-qPCR in astrocytes and microglia. As illustrated in Suppl Fig. 11B, we found that $CD8^+$ T cell depletion in mice raised in EE induced a significant decrease in expression level of Bdnf, Igf1 and Ntf5 in hippocampal astrocytes but not in microglia. $CD8^+$ T cell depletion in mice raised in SE induced no significant changes of expression of hippocampus Bdnf, Igf1 and Ntf5 neither in astrocytes nor in microglia. Thus, astrocytes could play a critical role as intermediates between the immune system and the brain plasticity.

ACCEPTED MANUSCRIPT

DISCUSSION

In this study, we show that $CD8^+$ T cells play a role in EE-induced effects on hippocampal plasticity and dependent behaviors. Although a role for $CD4^+$ T cells in brain plasticity has been described previously (Kipnis et al., 2008; Schwartz and Kipnis, 2011; Schwartz and Shechter, 2011), the involvement of $CD8^+$ T cells has never been demonstrated, to our knowledge, despite their presence in the brain in equal or even higher proportions compared to $CD4^+$ T cells in both rodents ((Song et al., 2016) and our data Suppl Fig 10, respectively) and humans (Loeffler et al., 2011; Smolders et al., 2013).

We found that $CD8^+$ T cell depletion blocked EE-induced neuronal proliferation and increased survival in the DG of the hippocampus. Neurogenesis has been largely shown to be under the control of several neurotrophic factors, in particular BDNF and IGF-1. In agreement, here we showed an increase in expression over time for Bdnf, Igf1, and to a lesser extent, the Ntf3 and Ntf5 genes in EE mice, which was abolished by $CD8^+$ T cell depletion.

$CD8^+$ T cell depletion also blocked the EE-induced synaptic changes in CA1 pyramidal neurons. Indeed, EE induced an increase in spine density measured at the basal dendrites of CA1 neurons. This response was in accordance with altered expression of CA genes that encode proteins which play a major role in the establishment of the glutamatergic synapse, both at the pre- and post-synaptic levels, including Bdnf gene expression. Interestingly, we also observed an increase in CX3CL1 (fractalkine) mRNA production, a chemokine known to be produced by neurons and acting on microglia to maintain a non-inflammatory state (Maggi et al., 2011). All of these changes were no longer present in $CD8^+$ T cell depleted mice.

The expression peak for most of the genes analyzed in DG and CA was often observed as rapidly as 2-3 weeks following transition to EE conditions. In future, it will be interesting to determine if shorter EE periods are sufficient to observe significant changes in the hippocampus.

ACCEPTED MANUSCRIPT

Our electrophysiological recordings performed in CA1 pyramidal neurons showed that the frequency of sEPSCs and mEPSCs was increased in EE compared to SE, while their mean amplitude or time constant of decay was unaffected by EE whereas we observed changes in morphology of the synapses (Fig. 4) and of post-synaptic protein expression levels in CA of the hippocampus (Fig. 5). This could be due to the fact that the synapses we analyzed morphologically are only a subset of the glutamatergic synapses reaching the CA1 neurons, whereas all glutamatergic inputs to CA1 pyramidal neurons were recorded electrophysiologically. The LTP amplitude was smaller in mice raised for 4 weeks in EE compared to SE as previously described (Hosseiny et al., 2015). This is likely due to a higher weight of excitatory synapses in EE compared to SE mice due to increased neuronal activity in hippocampus in EE mice. This increase in the strength of the excitatory synapses in EE would lead to a ceiling effect for EE mice when the HFS protocol is applied, whereas SE mouse synapses starting with a lower weight can be potentiated more. $CD8^+$ T cell depletion abolished all of these changes, suggesting that $CD8^+$ T cells also influence spinogenesis and that synaptic plasticity changes are triggered by EE in the hippocampus. It is interesting to note that the $CD8^+$ T cell depletion exerted some effects on synaptogenesis and the synaptic function of mice raised in SE. For instance, it significantly increased the head diameter (Fig 4B) and increased the sEPSC frequency without affecting the mEPSC frequency (Fig 6A). Therefore, $CD8^+$ T cells could impact the brain even in SE, but to a lesser extent than in EE.

Overall, our data suggest that $CD8^+$ T cell depletion blocked the EE-induced effects on hippocampal plasticity, and this correlated with the abolition of the beneficial effects on anxiety and spatial learning as revealed in behavioral tests that are known to involve the limbic system and particularly the hippocampus. $CD8^+$ T cell depletion had no effect on EE-induced changes in locomotion, resignation and social interactions.

Previous studies on central $CD4^+$ T cells suggested the requirement for brain antigen priming in T cell localization and function in the brain (Derecki et al., 2010). However, our results show that

ACCEPTED MANUSCRIPT

the EE-induced neurogenesis was still observed in OT-I mice (whose $CD8^+$ T cells express a specific-TCR directed against OVA, an antigen absent from the mice), suggesting that $CD8^+$ T cells can exert some effects on hippocampal plasticity by an antigen-independent mechanism. This is in agreement with recent data showing that effector-memory CD8+ T cells do not depend on TCR-signals to exert their regulatory functions. Indeed, effector-memory T cells migrate to peripheral tissues, including the brain, and some subpopulations have been shown to be associated with successful aging and cognitive functions (Arosa et al., 2016; Michel et al., 2016; Pereira and Akbar, 2016). However, in OT-1 mice, a small percentage of the T cells present an endogenous rearrangement of TCRs, which could drive the effects observed in CNS associated tissue.

T cells are present in the central nervous system, even under physiological conditions, both in rodents and humans (Loeffler et al., 2011; White et al., 2017). Interestingly, we and others have shown that the $CD4^+/CD8^+$ ratio among $CD3^+$ T cells was different in the whole brain compared to the blood and spleen suggesting selective attraction and/or retention of those cells in the brain (Suppl. Fig 10A and (Bradl et al., 2005; Ritzel et al., 2016; Smolders et al., 2013)). Moreover, we found that about 50% of the whole brain T cells ($CD3^+$ cells among $CD45^+$ $CD11b^-$ cells) are concentrated at the choroid plexus. Interestingly, choroid plexus from the lateral and third ventricles are lining the hippocampus, and T cells that are present there could influence hippocampal plasticity. However, no EE-dependent change was observed in the expression of genes involved in lymphocyte retention and trafficking at the choroid plexus level (data not shown).

FACS analysis of $CD8^+$ T cells revealed an increase in the $CD44^+$ $CD62L^{low}$ subpopulation (i.e. the effector memory subpopulation) in the whole brains of EE mice compared to SE mice, but the opposite was observed in the spleen. The $CD62L^{low}$ memory T cell population is a heterogeneous population including $CD69^+$ cells, known as “resident memory” (Farber et al., 2014; Mueller and Mackay, 2016). Their role under physiological conditions is yet to be elucidated, but in pathological conditions, they have been shown to play an important role in the brain (Park and Kupper, 2015;

ACCEPTED MANUSCRIPT

Steinbach et al., 2016). It will be interesting in the future to investigate their role in the hippocampal plasticity changes observed in EE.

EE housing affects $CD8^+$ T cell characteristics, both at peripheral and central levels. Indeed, by comparing splenic $CD8^+$ T cells of SE and EE mice, significant changes in gene expression were revealed by RNAseq analyses. IPA and GSEA analyses suggested that EE favors a $CD8^+$ T cell memory profile compared to SE housing. A similar approach has been used previously in naive $CD4^+$ and $CD8^+$ T cells sorted from spleens of young and aged mice, which also revealed some differences between the populations (Mirza et al., 2011). These results were consistent with the phenotypic characterization demonstrating that splenic $CD8^+$ T cells of mice raised in EE were more reactive to *in vitro* stimulation compared to those from mice raised in SE, including when they were stimulated by a TCR-independent mechanism (PMA-Iono). Indeed, $CD8^+$ T cells from EE released higher amounts of TNFα and proliferated more quickly, as revealed by CFSE-labeling (Fig 7).

We also compared the gene expression of a small population of $CD8^+$ T cells sorted from the choroid plexus of lateral and third ventricles of SE and EE housed mice, using a modified single-cell RNA sequencing technique. We found that genes were expressed differentially between SE and EE mice, confirming that whole brain $CD8^+$ T cells are modified by EE compared to SE. Interestingly, we found that very few genes that were modulated in EE in $CD8^+$ T cells from the whole brain were common with genes positively regulated in EE in $CD8^+$ T cells from the spleen, suggesting local modification pathways. It is important to note that in $CD8^+$ T cells from the choroid plexus, genes coding for TCR-linked signaling molecules (Lck, Lat), the MHCII-linked signaling molecule (Tagln2), and the cytokine receptor IL17rA were down-regulated. This suggests that central $CD8^+$ T cells adopt a profile that is less susceptible to activation in EE. Conversely, in the periphery we showed that peripheral $CD8^+$ T cells from spleen become more reactive in EE relative to SE upon stimulation, proliferating faster and releasing more cytokines as compared to SE $CD8^+$ T cells. This suggests that resident $CD8^+$ T cells in the brain and peripheral $CD8^+$ T cells behave differently in EE.

ACCEPTED MANUSCRIPT

This is consistent with recent findings showing that there is a resident population of "homing" $CD8^+$ T cells in the brain (Korin et al., 2017).

Various cytokines have been shown to participate in the recruitment of T cells from the periphery (Qi et al., 2017). One can hypothesize that the changes observed in $CD8^+$ T cells from the choroid plexus of EE *vs.* SE could be due to a variation in the concentration of factors locally released in the CSF by neurons or glial cells following increased synaptic activity in EE such as TGF-β, as GSEA analysis indicated TGF-β pathway activation in EE versus SE $CD8^+$ T cells of the choroid plexus.

Many questions remain to be elucidated. For instance, the respective contribution of peripheral *vs.* central $CD8^+$ T cells in EE-induced hippocampal changes needs to be clarified. Indeed, our depletion protocol affects both whole-brain and peripheral $CD8^+$ T cells and does not allow for the independent study of either of these two potentially different populations. The mechanisms by which $CD8^+$ T cells are affecting plasticity are also unknown. Since there is no direct physical contact between T cells and neurons in the brain parenchyma, the intercellular dialogue mediated by soluble molecules may involve cellular intermediates, which could be perivascular or meningeal macrophages, microglia, and/or astrocytes (Qi et al., 2017). We have obtained interesting data suggesting that in EE mice, astrocytes may serve as intermediates in the cascade linking EE-$CD8^+$ T cells to neuronal plasticity in hippocampus (Suppl Fig 11). Indeed, in EE, but not in SE, $CD8^+$ T cell depletion significantly decreased the expression of several trophic factor genes such as Bdnf, Igf1 and Ntf5, which are known to influence hippocampus plasticity (Aberg et al., 2003; Kang and Schuman, 1995). Microglia didn't seem to be affected but these points still are under investigation.

In conclusion, we demonstrated a major role of $CD8^+$ T cells on EE-induced hippocampal plasticity for the first time. $CD4^+$ T cells have been shown to be essential for correct brain function and plasticity (Kipnis et al., 2004b; Lewitus et al., 2007; Radjavi et al., 2014). Our work shows that $CD8^+$ T cells also contribute to optimal brain plasticity in EE conditions. Subtle phenotypic

ACCEPTED MANUSCRIPT

modifications of $CD8^+$ T cells in EE could promote neuronal plasticity directly or indirectly through astrocytes. Our study paves the way for the study of other immune cells, such as macrophages, mast cells and NK cells (Benaroya-Milshtein et al., 2004; Herz et al., 2017), which could also undergo changes in EE and participate in brain homeostasis and plasticity under non-pathological conditions.

ACCEPTED MANUSCRIPT

ACCEPTED MANUSCRIPT

FIGURE LEGENDS

Figure 1: $CD8^+$ T cell depletion affects EE-induced changes in hippocampal-dependent behavior.

A-E: Each dot represents an animal; values are means ± SEM.

A: $CD8^+$ T cell depleted mice housed for 4 weeks either in SE (white) or EE (grey) were tested for motor coordination, and assessed by the time of retention on the rotarod.

B: Mice were assessed in the open-field test (OF). Time spent in the aversive center of the arena (left) was compared to the number of entries in the center (right).

C: Anxiety behavior was assessed in the light/dark paradigm (L&D) by recording the number of attempts to go to light (left), the first entry in black (center) and the time spent in the lighted aversive area (right).

D-E: Anxiety and depressive-like phenotypes of $CD8^+$ T cells-depleted mice housed either in SE or EE were assessed by the latency to feed in the NSF (**D**) and the time of immobility in the FST (**E**). The NSF test was stopped after a 10 minute period.

F: Social skills were evaluated by the social interaction test: the % of time spent in the compartment previously associated with the presence of the mouse was measured as indicated. Means ± SEM, N=9 for each group.

G: Spatial learning curve was established by training in the Barnes maze for four consecutive days (two trainings a day). Groups were compared using the Friedman rank test for repeated measures with level of significance alpha fixed to 5% ($p < 0.0003$).

Dunn's multiple comparison	Difference in Rank Sum	*p* value	Significant
SE Ctrl vs EE Ctrl	13.00	$p < 0.05$	*
SE CD8 vs SE ctrl	9.00	$p > 0.05$	ns
SE CD8 ve EE CD8	13	$p < 0.05$	*
EE CD8 vs EE ctrl	9.00	$p > 0.05$	ns

H: Time spent in the target compartment during probe trials without the escape box conducted was evaluated at day 5 (D5) and day 9 (D9), t-test was performed on means. *: $p < 0.05$

ACCEPTED MANUSCRIPT

G and **H**: means ± SEM, N=10, 10, 10 and 14 for SE control, EE control, SE + anti CD8 Ab and EE + anti-CD8 Ab, respectively.

Figure 2: $CD8^+$ T cell depletion affects neurogenesis in DG of the hippocampus from SE and EE mice.

A: Chromogenic immunodetection of new $BrdU^+$ cells measured in the DG 24h (**a**) or 21 days after the first BrdU injection (**b-c**) in mice raised in SE (white) or EE (grey). WT mice were treated either with the depleting anti-CD8 antibodies mixture (see methods) or the control antibody mixture (**a, b**). **c**: Effect of 4 weeks in EE housing on the number of $BrdU^+$ cells in OT-I mice.

Each dot represents a mouse. Bars: means ± SEM. a,b: N= 6 per group. c: SE, N=7 and EE, N=13.

Two-way ANOVA	*p* interaction (treatment vs housing)	*p* treatment (Control vs Anti-CD8 Ab)	*p* housing (SE vs EE)
BrdU 24h	0.20	0.09	0.0146
BrdU 21j	0.0052	0.4002	0.0006

B: Confocal micrographs of the DG from control (left) or CD8 T cells-depleted (right) mice housed in SE (white) or EE (grey) showing the labeling of $BrdU^+$ (green) and $NeuN^+$ (red) cells (**a**). Histograms show the mean number of $BrdU^+$ cells and $BrdU^+$ $NeuN^+$ cells labeled in the DG (**b**).

Each dot represents a mouse. Bars: means ± SEM. N= 4 per group.

Figure 3: $CD8^+$ T cell depletion blocks EE-induced neurotrophic factor gene expression increase in the DG of the hippocampus.

DG were micro-dissected from hippocampus and transcript abundance of neurotrophic genes was determined by RT-qPCR after different housing duration (2W, 3W and 4W) in SE or EE conditions. Bars represent the mean expression levels ± SEM of the $2^{-\Delta\Delta Ct}$. For each gene, we first performed a

ACCEPTED MANUSCRIPT

Kruskal-Wallis test on the ΔCt values followed by an exact two-sample Fisher-Pitman permutation test comparing SE to EE at 3W and 4W, and comparing in each group (SE or EE) 3W to 1W and 4W to 1W in Fig 3A (or 3W to 2W and 4W to 2W for Ab-injected mice in Fig 3 B). The obtained p values were corrected using the FDR method of Benjamini-Hochberg for a total of 8 comparisons per gene. *: $p < 0.05$ and **: $p < 0.01$, N=6 for each group.

Figure 4: $CD8^+$ T cell depletion modifies EE-induced spinogenesis and dendritic spine morphology in CA1 neurons.

Spine characteristics were determined using NeuronStudio on segments of 45-50µm dendrites at the second basilar dendrites of CA1 neurons labeled with Alexa Fluor 568.

A- Number of spines/µm, B- Mean spine head diameter, C- Mean spine neck diameter, D- Mean spine length.

Bars are means ± SEM. SE is in white and EE is in grey. Statistical analysis was performed using two-way analysis of variance (ANOVA), followed by post-hoc t-test for comparison between groups for paired data. *: $p < 0.05$ and ***: $p < 0.001$.

	SE Control	EE control	SE $CD8^+$	EE $CD8^+$
Number of mice	4	4	6	6
Number of dendrites	83	82	105	106
Number of spines	1874	2841	2384	2856

Two-way ANOVA	*p* interaction (treatment vs housing)	*p* treatment (control vs anti-CD8 Ab)	*p* housing (SE vs EE)
Spine density	0.0645	0.0008	<0.0001
Spine head	<0.0001	<0.0001	0.0061
Spine neck	0.0319	<0.0001	0.6335
Spine length	<0.0001	<0.0001	<0.0001

Figure 5: $CD8^+$ T cell depletion blocks EE-induced expression increases for synaptic factor genes in the CA of the hippocampus.

ACCEPTED MANUSCRIPT

CA were micro-dissected from hippocampi and expression levels of genes involved in synapse activity and maturation was determined by RT-qPCR after different housing durations (1W, 2W, 3W and 4W) in SE or EE conditions. Bars represent the mean expression levels ± SEM of the $2^{-\Delta\Delta Ct}$. For each gene, we first performed a Kruskal-Wallis test on the ΔCt values followed by an exact two-sample Fisher-Pitman permutation test comparing SE to EE at 3W and 4W, and comparing in each group (SE or EE) 3W to 1W and 4W to 1W in Fig 5A (or 3W to 2W and 4W to 2W for Ab-injected mice in Fig 5 B). The obtained p values were corrected using the FDR method of Benjamini-Hochberg for a total of 8 comparisons per gene. *: $p < 0.05$, N=6 for each group.

Figure 6: $CD8^+$ T cell depletion modifies EE effects on spontaneous and miniature EPSPs and LTP at the CA3-CA1 synapse.

A: Histograms representing event frequency, event amplitude and the time constant of decay of spontaneous (left) and miniature (right) EPSCs recorded in pyramidal CA1 neurons by patch clamp in whole cell configuration. SE is in white, and EE is in grey. Number of slices and mice used are indicated on the top. *: $p < 0.05$, **: $p < 0.01$.

B: Field excitatory postsynaptic potentials (fEPSPs) recorded in the CA1 region of the hippocampus in response to a stimulation of Schaffer collaterals every 30 s. Stimulating intensity was chosen to trigger a fEPSP of 50 % of the maximum response. After a stable baseline of 20 min, the high-frequency stimulation (HFS) protocol was applied (100 Hz during 1 s). Then, the 30 s stimulation with the same intensity restarted and a potentiation of the response to the stimulation was observed as expected, to 125–300 % of the initial response. Curves show the time course of the slope amplitude of the EPSPs for an average of representative slices of each group of mice, a group raised for 8 weeks in SE, and a group raised for 4 weeks in EE since 4 weeks of age. LTP was established in both groups after the HFS, but its magnitude was less pronounced in the group of mice raised for 4 weeks in EE.

ACCEPTED MANUSCRIPT

C: Histograms showing the mean percentage of LTP (measured on the sEPSC slope) ± SEM obtained 40 min after HFS according to the different conditions. SE is in white and EE is in grey. Number of slices and mice used are indicated on the top. *: $p < 0.05$.

Figure 7: $CD8^+$ T cells from mice raised in SE or EE present different phenotypic characteristics.

A-B: EE enhances TNFα but not IFNγ secretion (measured by MSD) of $CD8^+$ T cells from spleen, either sorted (**A**) or enriched by negative selection (**B**) after a 72 h period of *in vitro* stimulation with CD3/CD28. Mean ± SEM, N=6 in each group.

C: EE enhances TNFα but not IFNγ secretion (measured by MSD) of sorted $CD8^+$ T cells from spleen, after a 4 h period of *in vitro* stimulation with PMA/iono. Mean ± SEM, N=8 in each group.

D-E: Representative FACS profiles of splenic CFSE-labeled $CD8^+$ T cells from SE (white) and EE (grey) mice (**D**) and percentage of proliferating $CD8^+$ T cells after a 72 h period of stimulation with CD28 and different concentrations of CD3 (**E**). Mean ± SEM, N=3 in each group.

Figure 8: Transcriptomic analysis of $CD8^+$ T cells from spleen of mice raised in EE and SE

A: MA-plot for the comparison between enriched and standard environment for $CD8^+$ T cells from spleen. X-axis: average gene expression levels measured as $\log_2$ UMI counts + 1. Y-axis: $\log_2$ fold-change between EE and SE. b Red dots: differentially expressed genes, selected based on a combination of $p < 0.01$, abs ($\log_2$ fold-change) >1 and average expression >2.

B: Gene expression levels of the 12 genes exhibiting the most significant differences between enriched and standard environments in $CD8^+$ T cells from spleen. Data are expressed as UMI counts.

Symbol	**BaseMean**	**log2FoldChange**	***p* Value**
Rmi1	2.08	2.09	0.00
Ascc2	2.98	2.07	0.00
Atmin	2.95	1.91	0.00
Trav9n.3	2.57	1.76	0.01
Qk	2.26	1.76	0.01

ACCEPTED MANUSCRIPT

Lpcat4	4.29	1.76	0.00
Casc4	2.06	-1.61	0.00
Det1	2.94	-1.65	0.01
Zfp865	3.70	-1.68	0.00
Ppp1r12b	2.73	-1.83	0.00
Nenf	2.38	-2.20	0.00
Carns1	2.06	-2.54	0.00

Note: candidate DEG selected using the following criteria:

$p < 0.01$, abs (log_2FoldChange) > 1, base Mean > 2

C: Heatmap of the top 50 most differentially expressed genes when comparing spleen $CD8^+$ T cells from enriched and standard environment. Expression levels were centered by genes. Hierarchical clustering of the samples and genes used Euclidean distance and complete linkage.

Figure 9: Transcriptomic analysis of choroid plexus $CD8^+$ T cells

A: MA-plot for the comparison between enriched and standard environments for $CD8^+$ T cells from plexus choroid. X-axis: average gene expression levels. Y-axis: log_2 fold-change between EE and SE. Red dots: $p < 0.05$

B: Gene expression levels of the 12 genes exhibiting the most significant differences between Enriched and Standard environments in $CD8^+$ T cells from plexus choroid ($p < 0.05$). Data are expressed as UMI counts.

Symbol	BaseMean	log2FoldChange	*p* Value
Cst3	6.92	0.88	0.01
Enpp2	18.00	0.82	0.01
Rpl19.ps1	5.21	0.68	0.03
Higd2a	2.66	0.66	0.05
Rps17	6.31	0.60	0.04
Lck	11.38	-0.57	0.05
Lat	9.33	-0.59	0.03
H2afz	7.55	-0.62	0.05
Gm9800	4.10	-0.70	0.05
Tuba1a	4.19	-0.76	0.02
Tagln2	4.80	-1.05	0.00

Note: Il17ra was added to the graph, the gene does not have a $p < 0.05$

ACCEPTED MANUSCRIPT

C: Heatmap of the top 50 most differentially expressed genes when comparing enriched and standard environment in $CD8^+$ T cells from plexus choroid. Expression levels were centered by genes. Hierarchical clustering of the samples and genes used Euclidean distance and complete linkage.

Figure 10: Phenotypic characterization of $CD8^+$ T cells from spleen and whole brain.

A-: **a-** Representative bivariate dot plots of isolated immune cells from spleen. $CD8^+$ T cells were gated based on $CD3^+$ $CD11b^-$ $CD4^-$expression and $CD62L^{high}$ and $CD62L^{low}$ cells were identified among $CD3^+$ $CD8^+$ $CD44^+$ cells.

b-c- Histograms representing the spleen count of cells according to CD62L expression for a representative mouse raised in SE **(b**) or EE (**c**).

B- a- Representative bivariate dot plots of Percoll isolated whole brain immune cells illustrating gating on $CD45^+/CD11b^-$ cells to exclude microglia. $CD8^+$ T cells were gated based on CD3 expression and $CD62L^{hi}$ and $CD62L^{low}$ cells were identified among $CD3^+$ $CD8^+$ $CD44^+$ cells.

b-c- Histograms representing the brain count of cells according to CD62L expression for a representative mouse raised in SE (**b**) or EE (**c**).

C-D: Percentages of $CD62L^{low}$ (**C**) and $CD62L^{high}$ (**D**) cells among splenic (left) and whole brain (right) $CD8^+$ $CD44^+$ T cells in SE and EE housed mice. Mean ± SEM for 3 independent experiments. Number of mice used is indicated on the top. SE in white, EE in grey. Statistical analysis was performed using two-way analysis of variance (ANOVA), followed by post-hoc t-test for comparison between groups for paired data. *: $p < 0.05$, **: $p < 0.01$, ***: $p < 0.001$

Two-way ANOVA	*p* interaction (treatment vs housing)	*p* treatment (control vs anti-CD8 Ab)	*p* housing (SE vs EE)
CD62L low (C)	0.0755	<0.0001	0.0003
CD62L high (D)	0.0877	<0.0001	0.0004

ACCEPTED MANUSCRIPT

SUPPLEMENTARY FIGURES

Supplementary Figure 1: Enrichment environment, depletion and behavioral test protocols.

A: 3W female mice were *ip* injected with anti-CD8 or isotype control antibodies 3 days before being placed in EE or maintained in SE. Mice received 2 other injections every 10 days to ensure complete depletion. For BrdU injections, mice were *ip* injected with BrdU once a day for 5 days. The first injection was performed 21 days before mice were euthanized.

B: Behavioral test protocol. Behavioral tests were carried out on the same mice from SE or EE housing injected with control or anti-CD8 antibodies, starting from the least (rotarod, L&D and open-field) to the most stressful tests (NSF, and FST).

C: 12-15 mice raised in an enriched environment (EE, right) were placed in large cages (9 120 cm2; L x l x h: 120 x 76 x 21 cm) equipped with nesting material, houses, running wheels, hammocks, scales, plastic toys and tunnels. Objects were changed twice a week. By contrast, standard environment (SE, left) consisted of middle-sized cages (666 cm2; L x l x h: 36 x 18.5 x 14 cm) with five mice/cage without objects.

D: $CD8^+$ T cell depletion did not impact the animal weigh measured after 4W housing in SE or EE.

Supplementary Figure 2:

A: Anti-CD8 antibody treatment is not sufficient to eliminate all $CD8^+$ T cells.

Plots representing blood CD4/CD8 profile gated on $CD45^+$ $CD3^+$ population (top) 3 days after an *ip* injection either of an anti-rat isotype antibody (control condition, left) or anti-CD8 (middle) or anti-rat secondary antibody-coupled anti-CD8 antibody (ratio 1:1, right). Middle panel shows that with the anti-CD8 injection, the CD8 epitope was saturated but $CD8^+$ T cells were still present. The using

ACCEPTED MANUSCRIPT

of a secondary antibody coupled anti-CD8 antibody was effective to deplete almost all $CD8^+$ T cells (right panels).

B: Using an anti-rat secondary antibody-coupled anti-CD8 depleting antibody eliminates $CD8^+$ T cells in whole brain. Plots representing CD4/CD8 whole brain profile gated on $CD45^+$ $CD11b^-$ $CD3^+$ cells 7 days after an *ip* injection either of control (left) or anti-CD8 (right) antibodies.

Supplementary Figure 3: $CD8^+$ T cell depletion affects mouse performances in the Barnes Maze test.

A: Map of the spatial organization of the Barnes maze. The black circle represents the location of the black Plexiglas box placed underneath as an escape chamber.

B, C: Histograms representing the time spent in the different areas delineated in A at day test 5 (D5) to evaluate the learning process (B) and at day 9 (D9) to evaluate the memory retention (C) for the various groups of mice indicated. * $p < 0.05$.

Supplementary Figure 4: Morphology of the dendrites and spines of injected CA1 neurons in fixed slices of the hippocampus of control and $CD8^+$ T cell depleted EE and SE mice.

A: representative photomicrographs of neurons in z projections and examples of dendrites at a higher magnification.

B: Example of analysis of a dendrite with the NeuronStudio software.

C: Repartition of the different dendritic spine types

D: Schematic representation of the spine types

Supplementary Figure 5: Effect of $CD8^+$ T cell depletion on cumulative histograms of spontaneous and miniature EPSPs.

ACCEPTED MANUSCRIPT

Condition	SE control sEPSCs	EE control sEPSCs	SE CD8 Ab sEPSCSs	EE CD8 Ab sEPSCs	SE control mEPSCs	EE control mEPSCs	SE CD8 Ab mEPSCs	EE CD8 Ab mEPSCs
Number of cells	8	11	10	11	5	9	9	6
Number of mice	4	5	5	5	3	4	5	4
Number of events	2596	2596	2411	2411	2015	2015	3431	3431

Kolmogorov-Smirnov test was performed to compare the distributions using the Clampfit software (Molecular Devices). K is indicated for the repartitions that were found significantly different with $p < 0.05$.

Supplementary Figure 6:

A: Splenic $CD4^+$ T cells from SE and EE mice did not differ in their ability to secrete TNFα or IFNγ after a 4h period of stimulation with PMA/iono (C, D).

B: $CD4^+$ T cells from SE and EE mice did not differ in their ability to proliferate after an anti-CD3/CD28 stimulation. Histograms represent the percentage of proliferating $CD4^+$ T cells 72 h after stimulation with CD28 and different concentrations of CD3.

C: The percentages of $CD62L^{low}$ (**G**) and $CD62L^{high}$ (**H**) among $CD44^+$ $CD11b^-$ $CD3^+$ $CD4^+$ $CD44^+$ cells from total brain and spleen did not vary.

Supplementary Figure 7: Comparison of transcriptomic profile of $CD8^+$ T cells vs. $CD4^+$ T cells from spleen and choroid plexus.

Hierarchical clustering of gene expression levels for $CD4^+$ and $CD8^+$ T cells samples collected from spleen (**A**) and plexus choroid (**B**) for SE and EE mice, based on the 50 highest expressed markers. Gene expression values were $\log_2$ transformed and scaled by gene. Hierarchical clustering of the data

ACCEPTED MANUSCRIPT

was performed using Pearson correlation distance for samples, and Euclidean distance for genes. Complete linkage was used for both sample and gene clustering.

Supplementary Figure 8: IPA analysis of genes expressed in $CD8^+$ T cells from the spleen (red bars) and the choroid plexus (blue bars) from EE mice *vs.* SE mice.

A: Canonical pathways associated with genes differentially expressed (*i.e.* increased or decreased) when comparing LT8 cells between enriched and standard environments. Bars represent the strength of the statistical significance.

B: Molecular functions associated with genes differentially expressed (*i.e.* increased or decreased) when comparing LT8 cells between enriched and standard environments. Bars represent the strength of the statistical significance.

Supplementary Figure 9: GSEA analysis of genes expressed in $CD8^+$ T cells from the spleen and the choroid plexus from EE mice vs. SE mice

A: Example of enrichment plot obtained from comparing to the immunology C7 set of data.

B: Top pathways for genes enriched in $CD8^+$ T cells from spleen with the higher NES and selected by their name (containing CD8, not CD4 or transfected) from EE mice *vs.* SE mice.

C: Top pathways for genes enriched in $CD8^+$ T cells from the choroid plexus with the higher NES and selected by their name (containing CD8, not CD4 or transfected) from EE mice *vs.* SE mice.

Supplementary Figure 10: Characteristics of T cells in the whole brains of SE and EE mice.

A: Number of $CD3^+$, $CD4^+$ and $CD8^+$ T cells among whole brain $CD45^+$ $CD11b^-$ cells (n=11 each) and ratio comparison of the $CD4^+$: $CD8^+$ in spleen vs. whole brain (n in parenthesis).

B: Immunocytochemistry of T cells in choroid plexus tissue. Actin in green, DAPI in blue to indicate the nuclei, CD3 in red to label the T cells.

ACCEPTED MANUSCRIPT

Supplementary Figure 11: $CD8^+$ T cell depletion affects astrocytes but not microglia neurotrophic factor gene expression.

A: In each group, Cx3cr1 fold change was significantly increased in microglia compared to astrocytes confirming that our selection method was efficient.

B: Relative level of the neurotrophic factor genes Bdnf, Igf1 and Ntf5 in astrocytes and microglia was determined by RT-qPCR in SE or EE conditions in mice treated with control or anti-CD8 depleting antibodies. Each dot represents two pooled hippocampi (N=4 for each group). Bars represent the mean expression levels ± SEM of the $2^{-\Delta\Delta Ct}$. Kruskal Wallis test for comparison between groups was performed on ΔCt values followed by an exact two-sample Fisher-Pitman permutation test comparing EE control to EE $CD8^+$ T cell depleted. * $p < 0.05$.

ACCEPTED MANUSCRIPT

ACCEPTED MANUSCRIPT

ACKNOWLEDGEMENTS

We wish to thank Lucien Relmy and Alain Barbot for their assistance in the animal care facility, Iris Grosjean and Sophie Abelanet from the imaging platform of IPMC, Delphine Debayle, Anne Sophie Gay from the proteomic platform of IPMC, Emilie Murris and Cathy Widmann for helpful discussions. We thank Abby Curtis from the UCA Office of International Scientific Visibility for comments on the English version of the manuscript. We also warmly thank Caroline Vieuille from ANASTATS and Thomas Lorivel for their help on statistical analyses. Hadi Zarif was financed by a Labex ICST (Ion Channel Science and Therapeutics) fellowship. This work was partly supported by Fondation de l'Avenir (AP-rm-16-011-Chabry). It was developed in close collaboration with the UCAGenomiX, the functional genomics platform of Nice Sophia Antipolis, a partner of the National Infrastructure France Génomique (ANR-10-INBS-09-03).

ACCEPTED MANUSCRIPT

ACCEPTED MANUSCRIPT

REFERENCES

Aberg, M.A., Aberg, N.D., Palmer, T.D., Alborn, A.M., Carlsson-Skwirut, C., Bang, P., Rosengren, L.E., Olsson, T., Gage, F.H., Eriksson, P.S., 2003. IGF-I has a direct proliferative effect in adult hippocampal progenitor cells. Molecular and cellular neurosciences 24, 23-40.

Arguel, M.J., LeBrigand, K., Paquet, A., Ruiz Garcia, S., Zaragosi, L.E., Barbry, P., Waldmann, R., 2017. A cost effective 5 selective single cell transcriptome profiling approach with improved UMI design. Nucleic acids research 45, e48.

Arosa, F.A., Esgalhado, A.J., Padrao, C.A., Cardoso, E.M., 2016. Divide, Conquer, and Sense: CD8+CD28- T Cells in Perspective. Front Immunol 7, 665.

Bailey, M.T., Kinsey, S.G., Padgett, D.A., Sheridan, J.F., Leblebicioglu, B., 2009. Social stress enhances IL-1beta and TNF-alpha production by Porphyromonas gingivalis lipopolysaccharide-stimulated CD11b+ cells. Physiology & behavior 98, 351-358.

Benaroya-Milshtein, N., Hollander, N., Apter, A., Kukulansky, T., Raz, N., Wilf, A., Yaniv, I., Pick, C.G., 2004. Environmental enrichment in mice decreases anxiety, attenuates stress responses and enhances natural killer cell activity. The European journal of neuroscience 20, 1341-1347.

Bradl, M., Bauer, J., Flugel, A., Wekerle, H., Lassmann, H., 2005. Complementary contribution of CD4 and CD8 T lymphocytes to T-cell infiltration of the intact and the degenerative spinal cord. The American journal of pathology 166, 1441-1450.

Brynskikh, A., Warren, T., Zhu, J., Kipnis, J., 2008. Adaptive immunity affects learning behavior in mice. Brain, behavior, and immunity 22, 861-869.

Cardona, A.E., Huang, D., Sasse, M.E., Ransohoff, R.M., 2006. Isolation of murine microglial cells for RNA analysis or flow cytometry. Nature protocols 1, 1947-1951.

Cazareth, J., Guyon, A., Heurteaux, C., Chabry, J., Petit-Paitel, A., 2014. Molecular and cellular neuroinflammatory status of mouse brain after systemic lipopolysaccharide challenge: importance of CCR2/CCL2 signaling. Journal of neuroinflammation 11, 132.

ACCEPTED MANUSCRIPT

Derecki, N.C., Cardani, A.N., Yang, C.H., Quinnies, K.M., Crihfield, A., Lynch, K.R., Kipnis, J., 2010. Regulation of learning and memory by meningeal immunity: a key role for IL-4. The Journal of experimental medicine 207, 1067-1080.

Donzis, E.J., Tronson, N.C., 2014. Modulation of learning and memory by cytokines: signaling mechanisms and long term consequences. Neurobiology of learning and memory 115, 68-77.

Farber, D.L., Yudanin, N.A., Restifo, N.P., 2014. Human memory T cells: generation, compartmentalization and homeostasis. Nature reviews. Immunology 14, 24-35.

Goldschmidt, T.J., Holmdahl, R., Klareskog, L., 1988. Depletion of murine T cells by in vivo monoclonal antibody treatment is enhanced by adding an autologous anti-rat kappa chain antibody. Journal of immunological methods 111, 219-226.

Hagihara, H., Toyama, K., Yamasaki, N., Miyakawa, T., 2009. Dissection of hippocampal dentate gyrus from adult mouse. J Vis Exp.

Herz, J., Filiano, A.J., Smith, A., Yogev, N., Kipnis, J., 2017. Myeloid Cells in the Central Nervous System. Immunity 46, 943-956.

Heurteaux, C., Lucas, G., Guy, N., El Yacoubi, M., Thummler, S., Peng, X.D., Noble, F., Blondeau, N., Widmann, C., Borsotto, M., Gobbi, G., Vaugeois, J.M., Debonnel, G., Lazdunski, M., 2006. Deletion of the background potassium channel TREK-1 results in a depression-resistant phenotype. Nature neuroscience 9, 1134-1141.

Hosseiny, S., Pietri, M., Petit-Paitel, A., Zarif, H., Heurteaux, C., Chabry, J., Guyon, A., 2015. Differential neuronal plasticity in mouse hippocampus associated with various periods of enriched environment during postnatal development. Brain Struct Funct 220, 3435-3448.

Kang, H., Schuman, E.M., 1995. Long-lasting neurotrophin-induced enhancement of synaptic transmission in the adult hippocampus. Science 267, 1658-1662.

Kempermann, G., Kuhn, H.G., Gage, F.H., 1997. More hippocampal neurons in adult mice living in an enriched environment. Nature 386, 493-495.

ACCEPTED MANUSCRIPT

Kinsey, S.G., Bailey, M.T., Sheridan, J.F., Padgett, D.A., Avitsur, R., 2007. Repeated social defeat causes increased anxiety-like behavior and alters splenocyte function in C57BL/6 and CD-1 mice. Brain, behavior, and immunity 21, 458-466.

Kipnis, J., Avidan, H., Caspi, R.R., Schwartz, M., 2004a. Dual effect of CD4+CD25+ regulatory T cells in neurodegeneration: a dialogue with microglia. Proceedings of the National Academy of Sciences of the United States of America 101 Suppl 2, 14663-14669.

Kipnis, J., Cohen, H., Cardon, M., Ziv, Y., Schwartz, M., 2004b. T cell deficiency leads to cognitive dysfunction: implications for therapeutic vaccination for schizophrenia and other psychiatric conditions. Proceedings of the National Academy of Sciences of the United States of America 101, 8180-8185.

Kipnis, J., Derecki, N.C., Yang, C., Scrable, H., 2008. Immunity and cognition: what do age-related dementia, HIV-dementia and 'chemo-brain' have in common? Trends Immunol 29, 455-463.

Korin, B., Ben-Shaanan, T.L., Schiller, M., Dubovik, T., Azulay-Debby, H., Boshnak, N.T., Koren, T., Rolls, A., 2017. High-dimensional, single-cell characterization of the brain's immune compartment. Nature neuroscience.

Krueger, J.M., Obal, F.J., Fang, J., Kubota, T., Taishi, P., 2001. The role of cytokines in physiological sleep regulation. Annals of the New York Academy of Sciences 933, 211-221.

Lewitus, G.M., Zhu, J., Xiong, H., Hallworth, R., Kipnis, J., 2007. CD4(+)CD25(-) effector T-cells inhibit hippocampal long-term potentiation in vitro. The European journal of neuroscience 26, 1399-1406.

Loeffler, C., Dietz, K., Schleich, A., Schlaszus, H., Stoll, M., Meyermann, R., Mittelbronn, M., 2011. Immune surveillance of the normal human CNS takes place in dependence of the locoregional blood-brain barrier configuration and is mainly performed by CD3(+)/CD8(+) lymphocytes. Neuropathology 31, 230-238.

ACCEPTED MANUSCRIPT

Love, M.I., Huber, W., Anders, S., 2014. Moderated estimation of fold change and dispersion for RNA-seq data with DESeq2. Genome biology 15, 550.

Macosko, E.Z., Basu, A., Satija, R., Nemesh, J., Shekhar, K., Goldman, M., Tirosh, I., Bialas, A.R., Kamitaki, N., Martersteck, E.M., Trombetta, J.J., Weitz, D.A., Sanes, J.R., Shalek, A.K., Regev, A., McCarroll, S.A., 2015. Highly Parallel Genome-wide Expression Profiling of Individual Cells Using Nanoliter Droplets. Cell 161, 1202-1214.

Maggi, L., Scianni, M., Branchi, I., D'Andrea, I., Lauro, C., Limatola, C., 2011. CX(3)CR1 deficiency alters hippocampal-dependent plasticity phenomena blunting the effects of enriched environment. Frontiers in cellular neuroscience 5, 22.

Michel, J.J., Griffin, P., Vallejo, A.N., 2016. Functionally Diverse NK-Like T Cells Are Effectors and Predictors of Successful Aging. Front Immunol 7, 530.

Mirza, N., Pollock, K., Hoelzinger, D.B., Dominguez, A.L., Lustgarten, J., 2011. Comparative kinetic analyses of gene profiles of naive CD4+ and CD8+ T cells from young and old animals reveal novel age-related alterations. Aging cell 10, 853-867.

Moy, S.S., Nadler, J.J., Perez, A., Barbaro, R.P., Johns, J.M., Magnuson, T.R., Piven, J., Crawley, J.N., 2004. Sociability and preference for social novelty in five inbred strains: an approach to assess autistic-like behavior in mice. Genes, brain, and behavior 3, 287-302.

Mueller, S.N., Mackay, L.K., 2016. Tissue-resident memory T cells: local specialists in immune defence. Nature reviews. Immunology 16, 79-89.

Opp, M.R., 2005. Cytokines and sleep. Sleep medicine reviews 9, 355-364.

Park, C.O., Kupper, T.S., 2015. The emerging role of resident memory T cells in protective immunity and inflammatory disease. Nature medicine 21, 688-697.

Pechnick, R.N., Chesnokova, V.M., Kariagina, A., Price, S., Bresee, C.J., Poland, R.E., 2004. Reduced immobility in the forced swim test in mice with a targeted deletion of the leukemia

ACCEPTED MANUSCRIPT

inhibitory factor (LIF) gene. Neuropsychopharmacology : official publication of the American College of Neuropsychopharmacology 29, 770-776.

Pereira, B.I., Akbar, A.N., 2016. Convergence of Innate and Adaptive Immunity during Human Aging. Front Immunol 7, 445.

Peters, A., Kaiserman-Abramof, I.R., 1970. The small pyramidal neuron of the rat cerebral cortex. The perikaryon, dendrites and spines. Am J Anat 127, 321-355.

Picelli, S., Faridani, O.R., Bjorklund, A.K., Winberg, G., Sagasser, S., Sandberg, R., 2014. Full-length RNA-seq from single cells using Smart-seq2. Nature protocols 9, 171-181.

Porsolt, R.D., Bertin, A., Jalfre, M., 1977. Behavioral despair in mice: a primary screening test for antidepressants. Arch Int Pharmacodyn Ther 229, 327-336.

Qi, F., Zuo, Z., Yang, J., Hu, S., Yang, Y., Yuan, Q., Zou, J., Guo, K., Yao, Z., 2017. Combined effect of BCG vaccination and enriched environment promote neurogenesis and spatial cognition via a shift in meningeal macrophage M2 polarization. J Neuroinflammation 14, 32.

Radjavi, A., Smirnov, I., Kipnis, J., 2014. Brain antigen-reactive CD4+ T cells are sufficient to support learning behavior in mice with limited T cell repertoire. Brain, behavior, and immunity 35, 58-63.

Ritzel, R.M., Crapser, J., Patel, A.R., Verma, R., Grenier, J.M., Chauhan, A., Jellison, E.R., McCullough, L.D., 2016. Age-Associated Resident Memory CD8 T Cells in the Central Nervous System Are Primed To Potentiate Inflammation after Ischemic Brain Injury. Journal of immunology 196, 3318-3330.

Ron-Harel, N., Segev, Y., Lewitus, G.M., Cardon, M., Ziv, Y., Netanely, D., Jacob-Hirsch, J., Amariglio, N., Rechavi, G., Domany, E., Schwartz, M., 2008. Age-dependent spatial memory loss can be partially restored by immune activation. Rejuvenation research 11, 903-913.

Schwartz, M., Kipnis, J., 2011. A conceptual revolution in the relationships between the brain and immunity. Brain, behavior, and immunity 25, 817-819.

ACCEPTED MANUSCRIPT

Schwartz, M., Shechter, R., 2011. Protective autoimmunity functions by intracranial immunosurveillance to support the mind: The missing link between health and disease. Mol Psychiatry 15, 342-354.

Smolders, J., Remmerswaal, E.B., Schuurman, K.G., Melief, J., van Eden, C.G., van Lier, R.A., Huitinga, I., Hamann, J., 2013. Characteristics of differentiated CD8(+) and CD4 (+) T cells present in the human brain. Acta neuropathologica 126, 525-535.

Song, C., Nicholson, J.D., Clark, S.M., Li, X., Keegan, A.D., Tonelli, L.H., 2016. Expansion of brain T cells in homeostatic conditions in lymphopenic Rag2(-/-) mice. Brain, behavior, and immunity 57, 161-172.

Steinbach, K., Vincenti, I., Kreutzfeldt, M., Page, N., Muschaweckh, A., Wagner, I., Drexler, I., Pinschewer, D., Korn, T., Merkler, D., 2016. Brain-resident memory T cells represent an autonomous cytotoxic barrier to viral infection. The Journal of experimental medicine 213, 1571-1587.

Tough, D.F., 2003. Deciphering the relationship between central and effector memory CD8+ T cells. Trends Immunol 24, 404-407.

Vitkovic, L., Bockaert, J., Jacque, C., 2000. "Inflammatory" cytokines: neuromodulators in normal brain? Journal of neurochemistry 74, 457-471.

White, J.T., Cross, E.W., Kedl, R.M., 2017. Antigen-inexperienced memory CD8+ T cells: where they come from and why we need them. Nature reviews. Immunology 17, 391-400.

Wohleb, E.S., Hanke, M.L., Corona, A.W., Powell, N.D., Stiner, L.M., Bailey, M.T., Nelson, R.J., Godbout, J.P., Sheridan, J.F., 2011. beta-Adrenergic receptor antagonism prevents anxiety-like behavior and microglial reactivity induced by repeated social defeat. The Journal of neuroscience : the official journal of the Society for Neuroscience 31, 6277-6288.

Wojtowicz, J.M., Kee, N., 2006. BrdU assay for neurogenesis in rodents. Nature protocols 1, 1399-1405.

ACCEPTED MANUSCRIPT

Wolf, G., Yirmiya, R., Goshen, I., Iverfeldt, K., Holmlund, L., Takeda, K., Shavit, Y., 2003. Impairment of interleukin-1 (IL-1) signaling reduces basal pain sensitivity in mice: genetic, pharmacological and developmental aspects. Pain 104, 471-480.

Yirmiya, R., Goshen, I., 2011. Immune modulation of learning, memory, neural plasticity and neurogenesis. Brain, behavior, and immunity 25, 181-213.

ACCEPTED MANUSCRIPT

ACCEPTED MANUSCRIPT

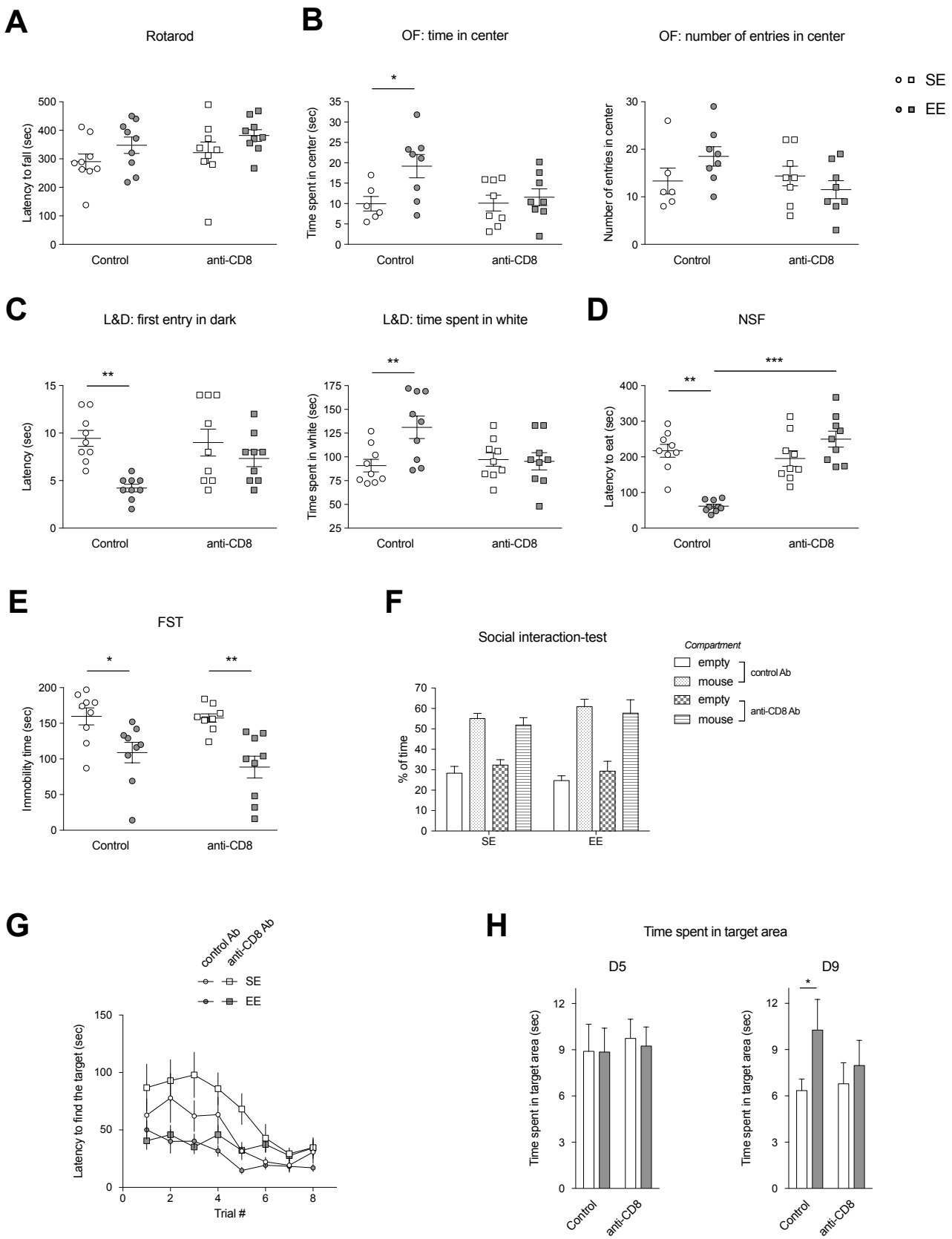

Figure 1

ACCEPTED MANUSCRIPT

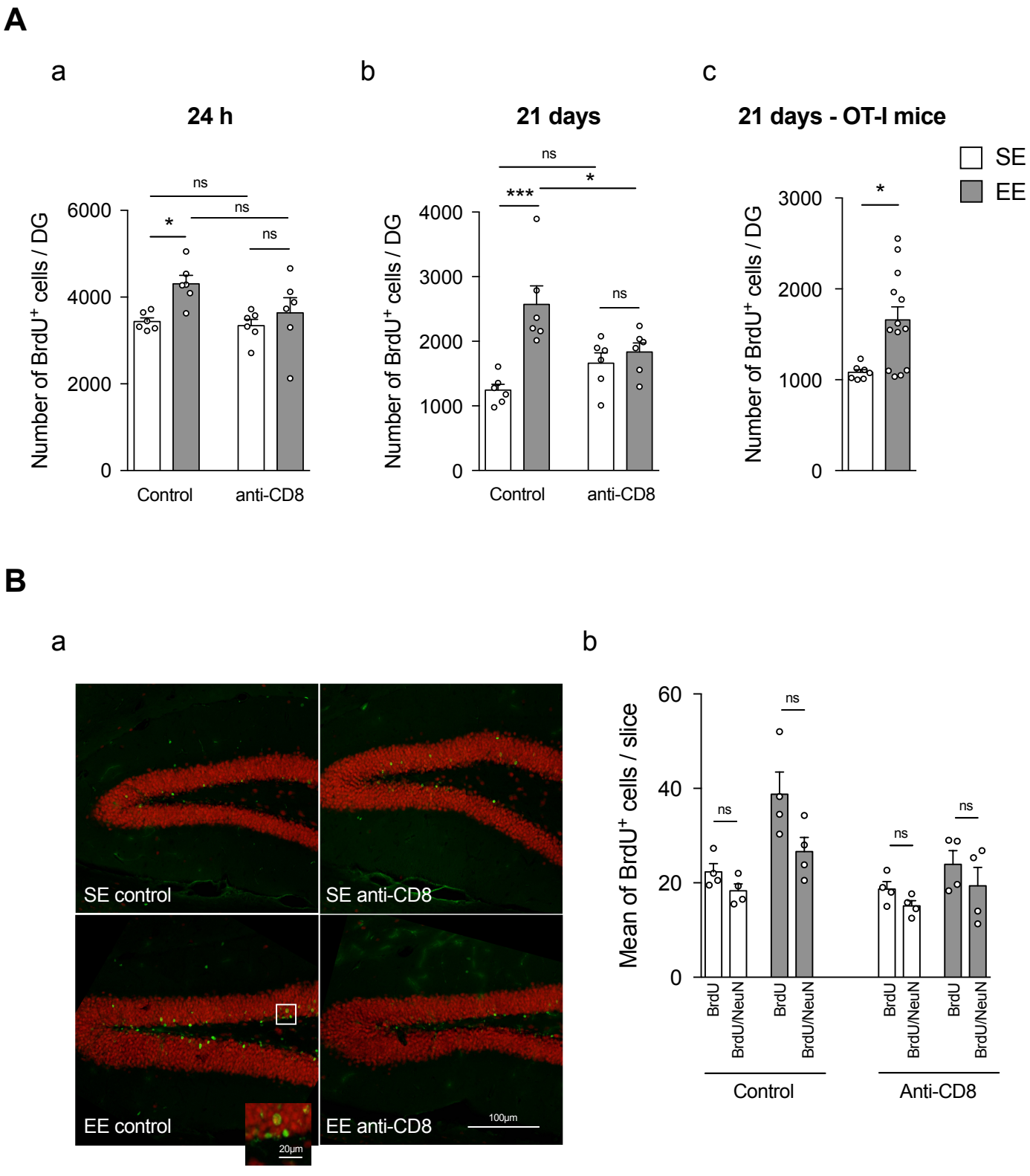

Figure 2

ACCEPTED MANUSCRIPT

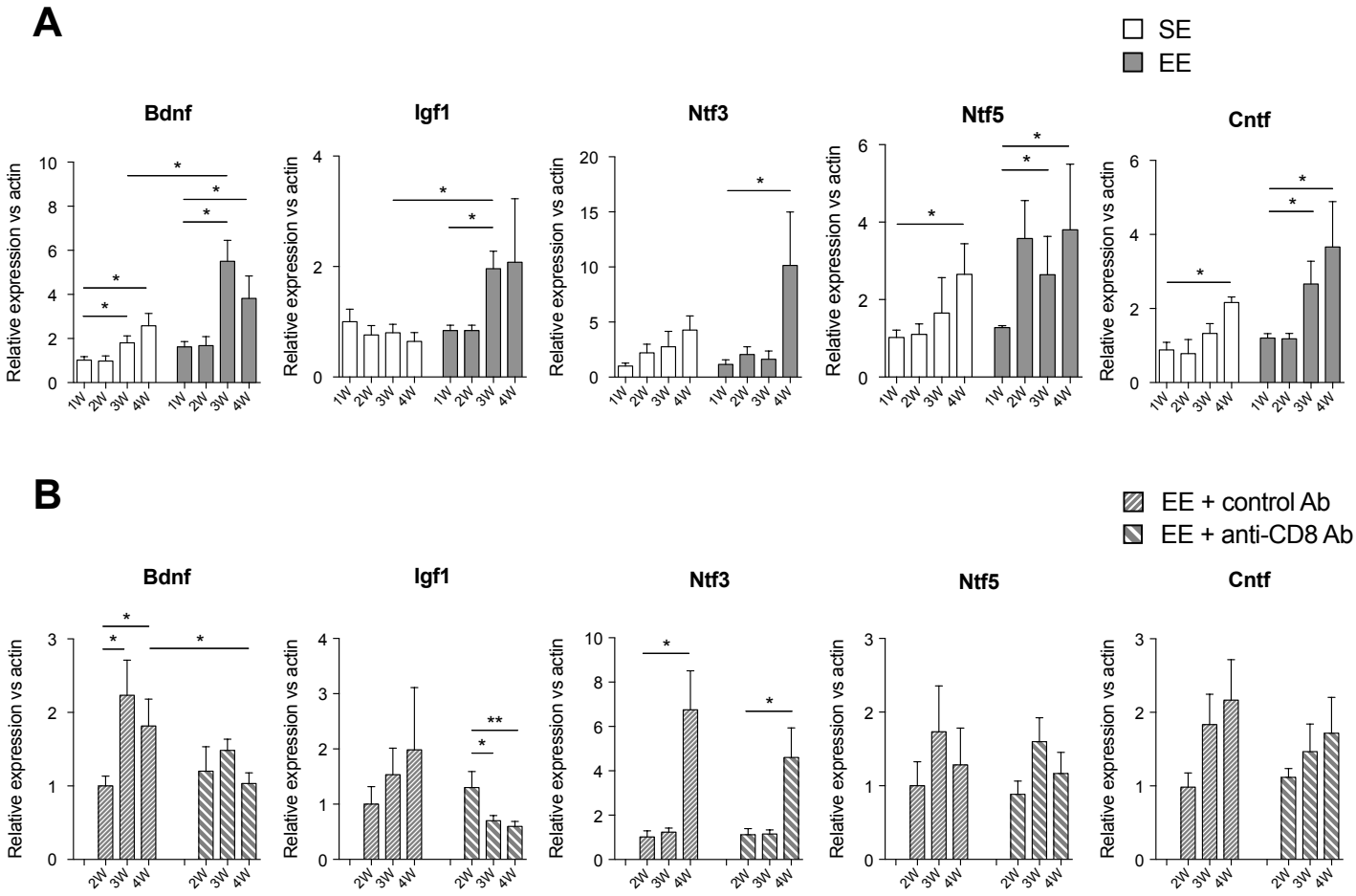

Figure 3

ACCEPTED MANUSCRIPT

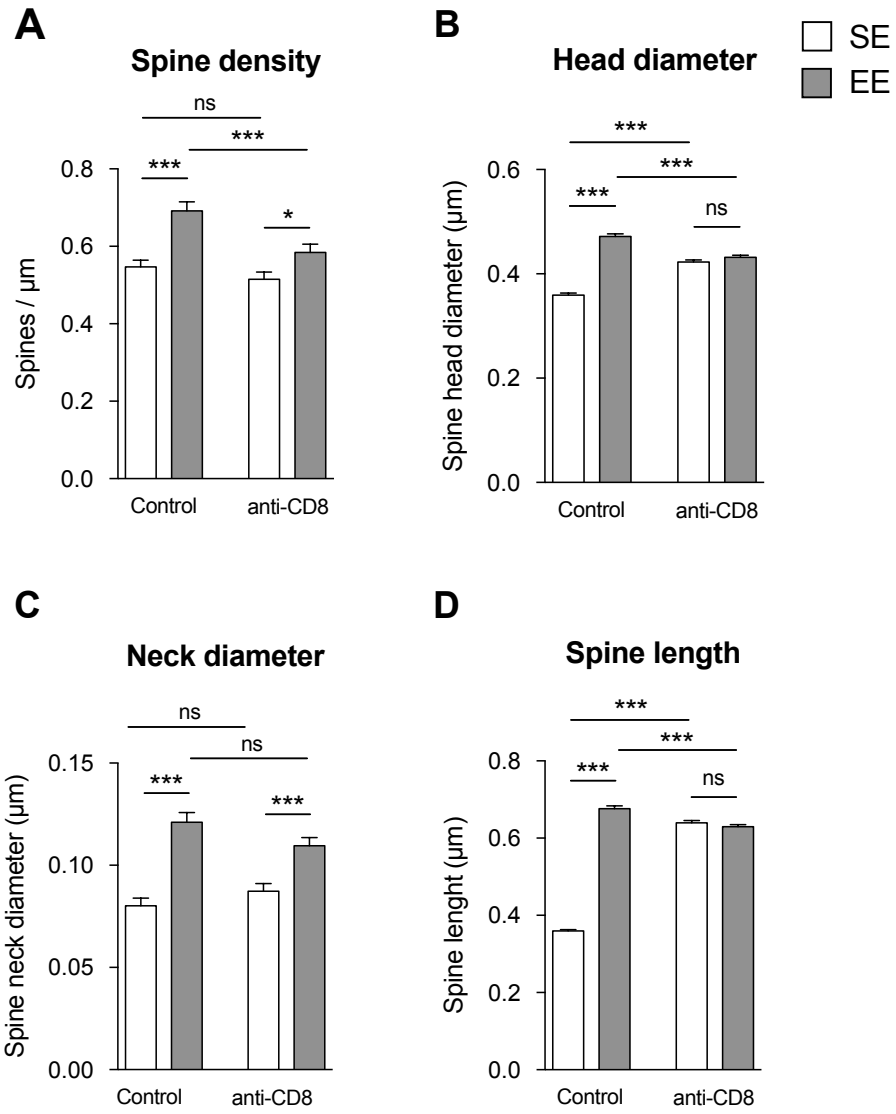

Figure 4

ACCEPTED MANUSCRIPT

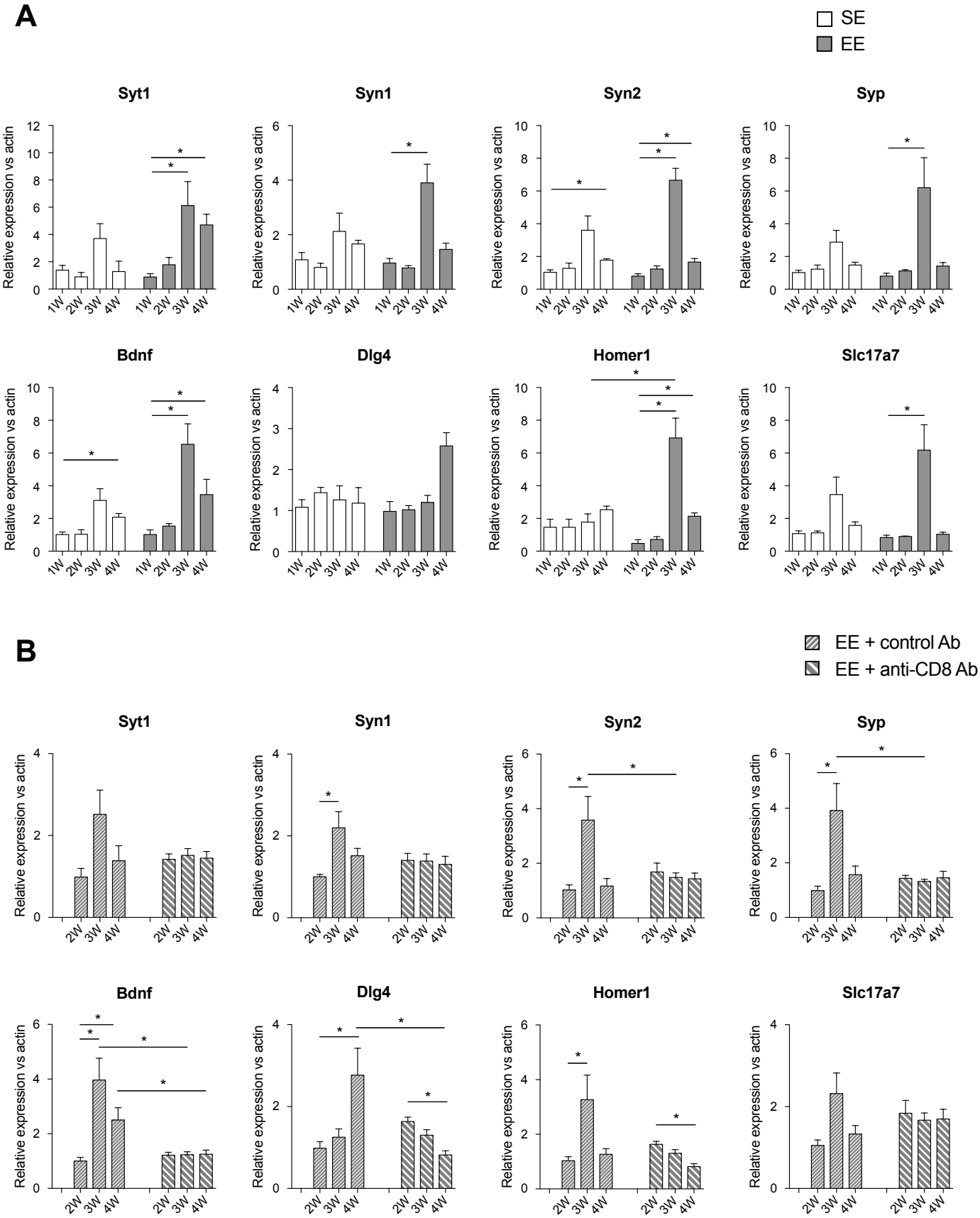

Figure 5

ACCEPTED MANUSCRIPT

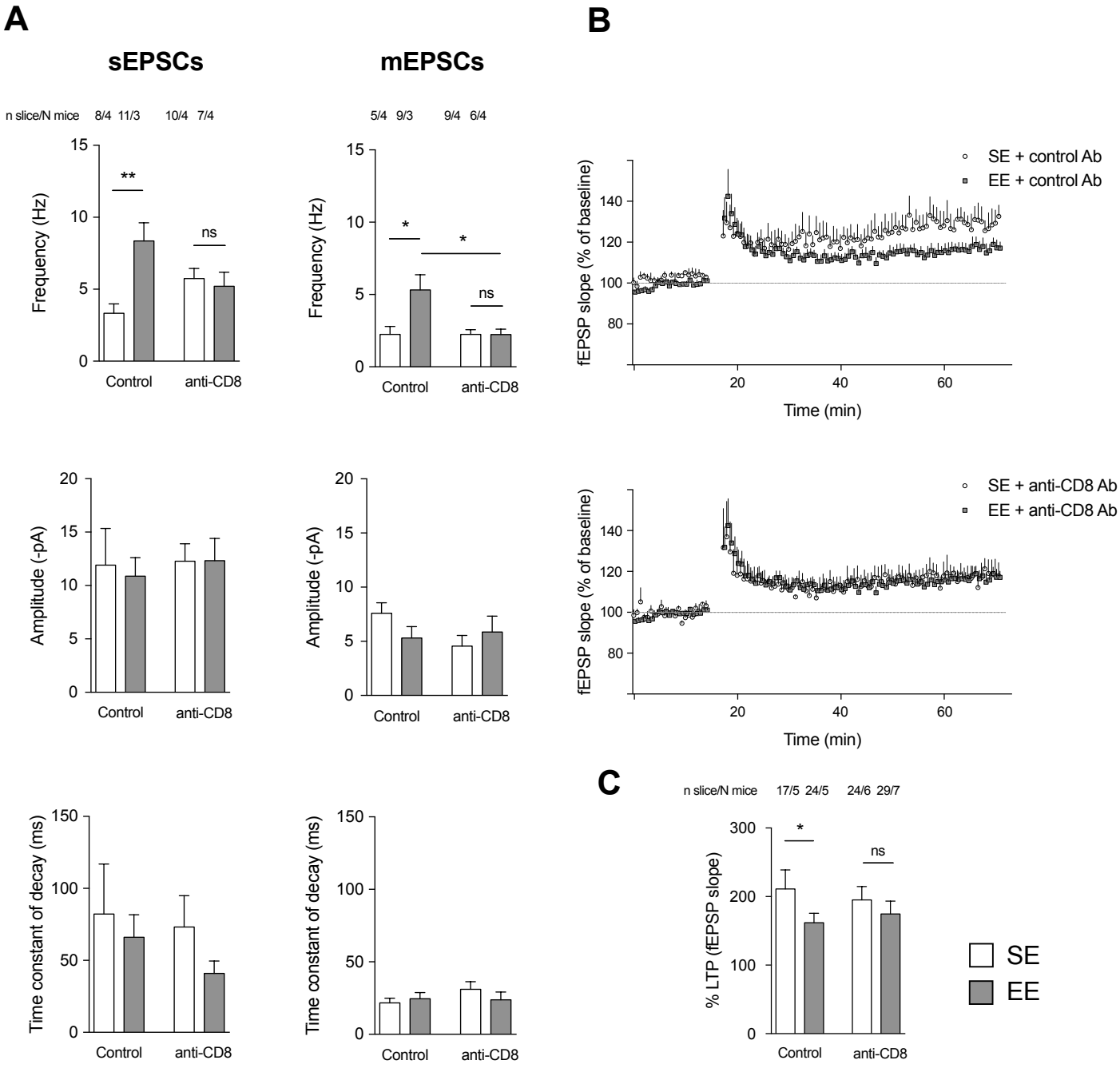

Figure 6

ACCEPTED MANUSCRIPT

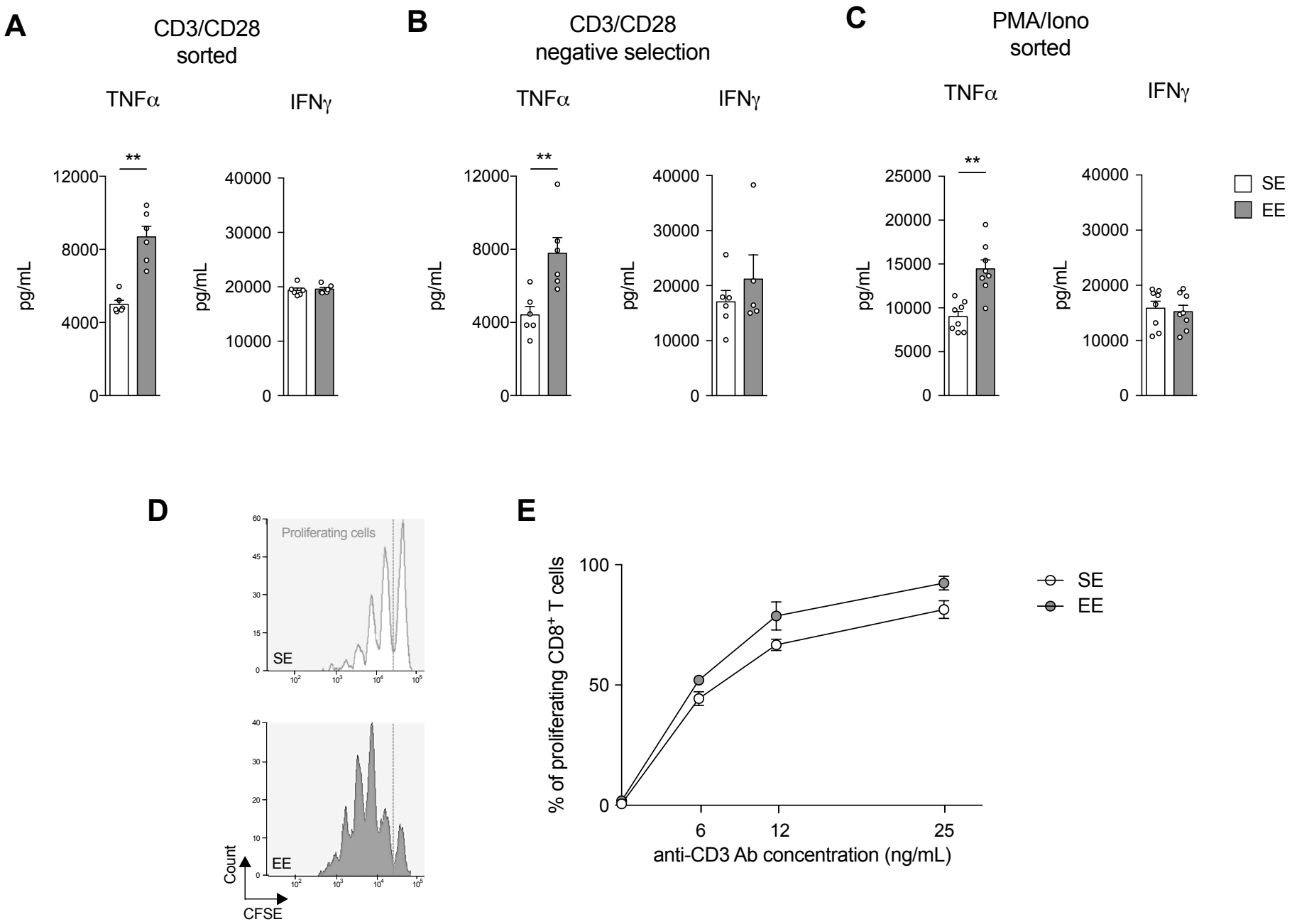

Figure 7

ACCEPTED MANUSCRIPT

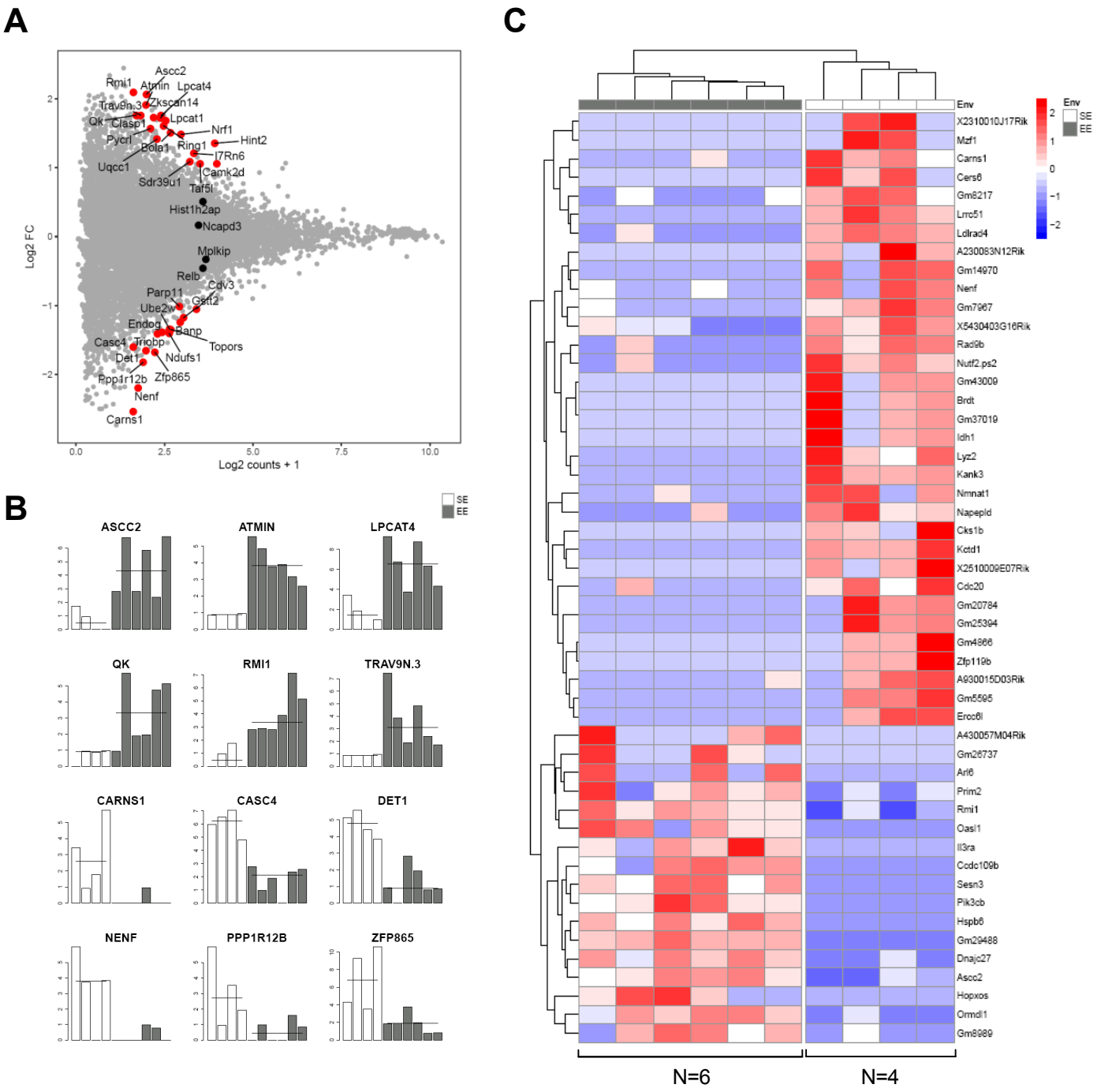

Figure 8

ACCEPTED MANUSCRIPT

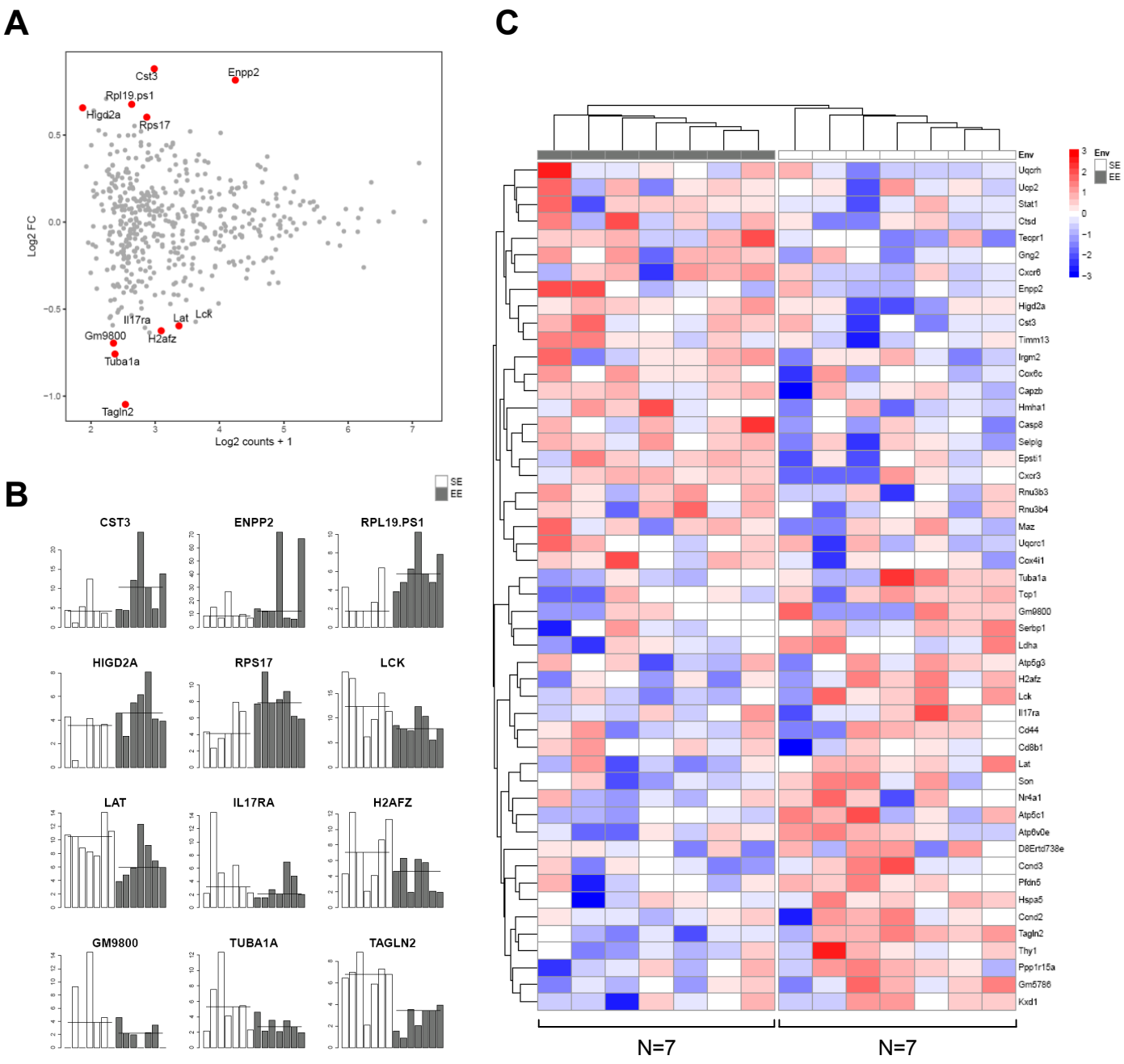

Figure 9

ACCEPTED MANUSCRIPT

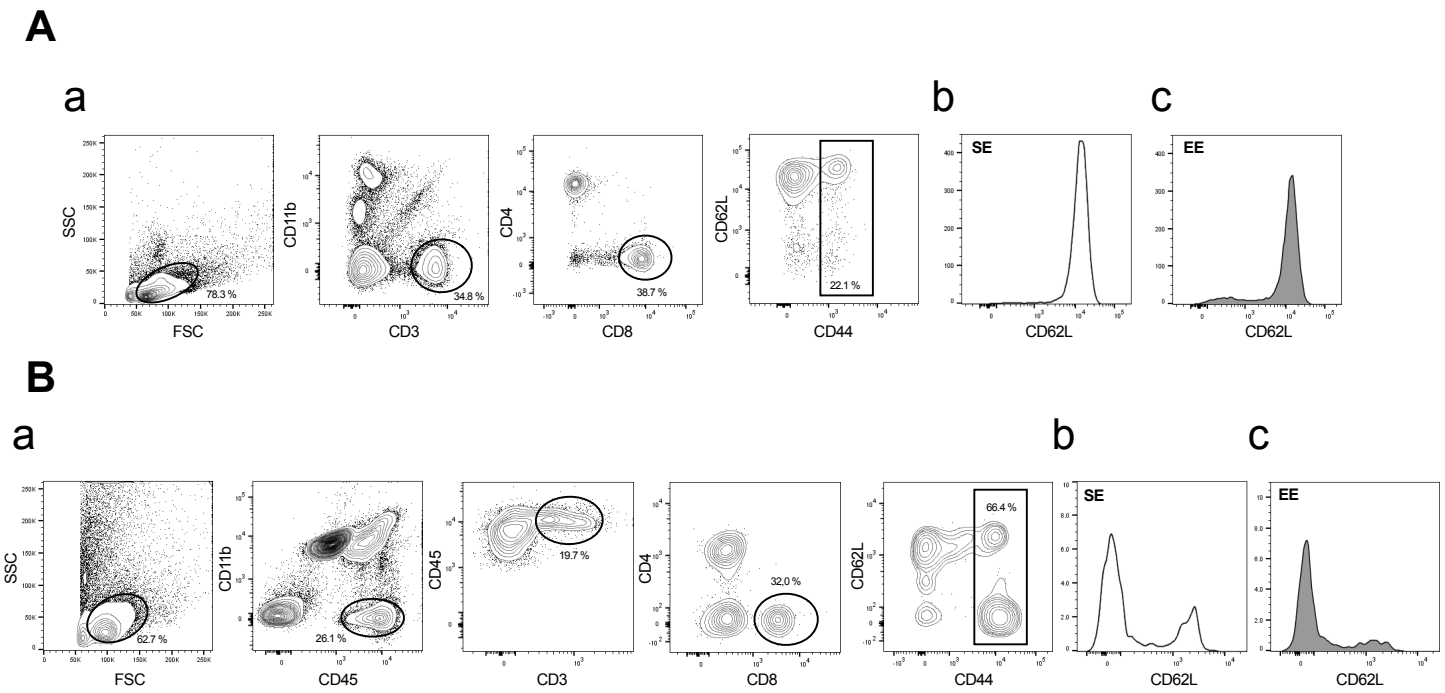

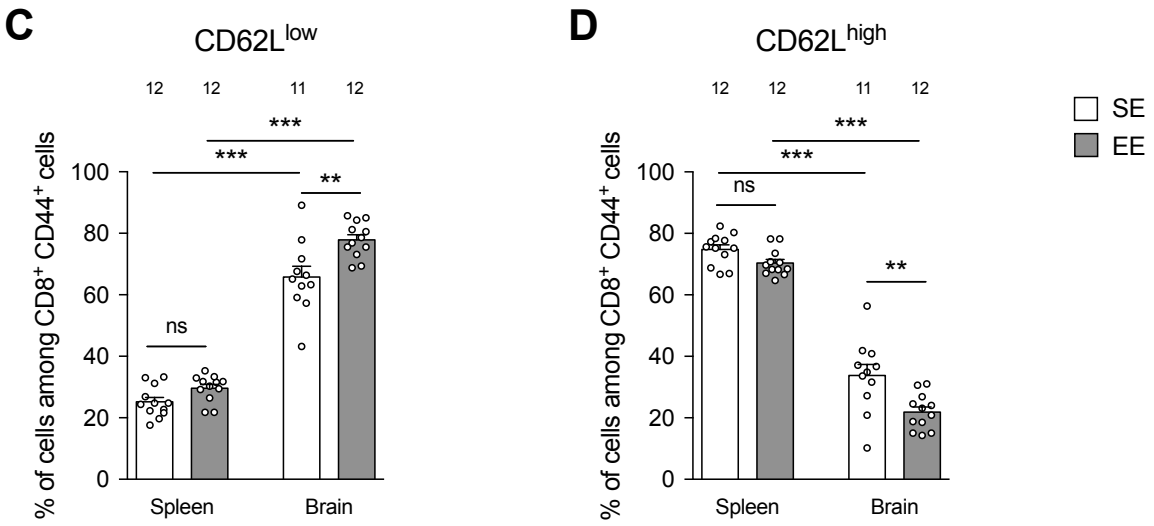

Figure 10

ACCEPTED MANUSCRIPT

Highlights:

- $CD8^+$ T cells play a major role in brain plasticity changes that are induced by an enriched environment in mice, as revealed by behavioral experiments and measurements of hippocampal volume, neurogenesis in the dentate gyrus of the hippocampus, spinogenesis and glutamatergic synaptic function in cornu ammonis (CA) of the hippocampus.

- Peripheral $CD8^+$ T cells have different properties in mice raised in an enriched environment (EE) as compared to mice raised in a standard environment (SE). Spleen $CD8^+$ T cells from SE vs EE mice are different in terms of 1) cytokine release after *in vitro* stimulation 2) *in vitro* proliferation properties 3) $CD44^+$ $CD8^+$ $CD62L^{low}$ and $CD62L^{hi}$ T cell proportions and 4) transcriptomic signature as revealed by RNA sequencing.

- $CD8^+$ T cell ratios and repartition of effector and central memory $CD8^+$ T cells differ between spleen and brain. Brain $CD8^+$ T cell transcriptomic signatures are differentially modified by EE housing, in comparison to peripheral $CD8^+$ T cells.

ACCEPTED MANUSCRIPT